Crystal and cryo-EM structures of the cytosolic G protein alpha chaperone and guanine nucleotide exchange factor Ric-8A bound to Gαi1

Levi J. McClelland[1*], Kaiming Zhang[4 *], Tung-Chung Mou[1,3*], Jake Johnston[1,3], Cindee Yates-Hansen[1], Shanshan Li[4], Celestine J. Thomas[1,†], Tzanko I. Doukov[6], Sarah Triest[7,8], Alexandre Wohlkonig[7,8], Gregory G. Tall[9], Jan Steyaert[7,8], Wah Chiu[2,5] and Stephen R. Sprang[1,2,3]

Affilliations

[1]Center for Biomolecular Structure and Dynamics, University of Montana, Missoula, MT, USA

[2]Graduate Program in Biochemistry and Biophysics, University of Montana, Missoula, MT, USA

[3]Division of Biological Sciences,University of Montana, Missoula, MT, USA

[4]Departments of Bioengineering and James H. Clark Center, Stanford University, Stanford, CA, USA

[5]Biosciences Division, SLAC National Accelerator Laboratory, Stanford University, Menlo Park, CA, USA

[6]Macromolecular Crystallography Group, Stanford Synchrotron Radiation Light Source, SLAC National Accelerator Laboratory, Stanford University, Stanford, CA, USA

[7]Structural Biology Brussels, Vrije Universiteit Brussel (VUB), Brussels, Belgium.

[8]VIB-VUB Center for Structural Biology, VIB, Brussels, Belgium.

[9]Department of Pharmacology, University of Michigan Medical School, Ann Arbor, MI, USA

† Present address, Regeneron Pharmaceutical, Inc. USA

Ric-8A is a cytosolic Guanine Nucleotide exchange Factor (GEF) that activates heterotrimeric G protein alpha subunits (Gα)[1]. Ric-8A is essential to life in multicellular eukaryotes by virtue of its chaperone activity that is required for Gα biogenesis and membrane localization[2,3]. Ric-8A adopts an armadillo (ARM)/HEAT repeat domain architecture and is structurally unrelated to G Protein-Coupled Receptors (GPCR)[4]. Both GEF and chaperone activities are stimulated by Casein Kinase II phosphorylation[5]. The mechanisms by which Ric-8A catalyzes GDP release and GTP binding to Gα, or exerts chaperone activity are unknown. Here, we report the structure of the nanobody-stabilized complex of nucleotide-free Gαi1 (isoform 1 of Gα family i) and phosphorylated Ric-8A at near atomic resolution by cryo-electron microscopy and X-ray crystallography. We find that Ric-8A envelops the GTPase domain of Gα, disrupting all three switch regions that convey Gα nucleotide-binding and signaling activity, and displaces the C-terminal helix and helical domain of Gα. These cooperative interactions dismantle the GDP binding site and promote GDP release, while protecting structural elements of Gα that are dynamic in the nucleotide-free state. The structures also show how *in vivo* phosphorylation stabilizes Gα-binding elements of Ric-8A, thereby enhancing its GEF and chaperone activities.

Genetic[6-8] and biochemical data[9] support a role for Ric-8A in G protein-coupled receptor (GPCR)-independent regulation of asymmetric cell division that is essential for embryonic development[10]. Ric-8A exhibits GEF and chaperone activity towards G protein alpha subunits (Gα) of the I, q and 12/13 classes[1], while Ric-8B, performs these functions for Gαs and Gαolf - each in a variety of cellular contexts[11,12]. That the Gα-class specificity of Ric-8A and Ric-8B is the same for GEF and chaperone activities[13] suggests a common mechanistic basis for both.

52 Biophysical data show that nucleotide-free Gαi1 is structurally dynamic when bound to
53 Ric-8A[14,15] and shares some properties with GPCR-bound Gα[16]. Namely, Ric-8A
54 induces rotational dynamics in the Gα helical domain[17] and binds to the C-terminus of
55 Gα [14,18]. In contrast to GPCRs, there is evidence that Ric-8A forms extensive
56 interactions with the Gα switch regions that undergo GTP-dependent conformational
57 changes[1,15,18,19] and with the Gα β-sheet scaffold[15].

58 To better understand the structural basis of Ric-8A GEF and chaperone activity, we
59 have determined the structure of the Ric-8A:Gαi1 complex, using both cryo-electron
60 microscopy (cryo-EM) and X-ray crystallography. To form the complex we used the N-
61 terminal 491-residue fragment of rat Ric-8A, which is a more active GEF then the full-
62 length (530 amino acid) protein, and, to reduce conformational heterogeneity, we used
63 the N-terminal 31-residue truncation mutant of rat Gαi1 (Δ31NGαi1), an efficacious
64 substrate for Ric-8A[14]. Recombinant Ric-8A(1-491) was phosphorylated by Casein
65 Kinase II at S435 and T440, which is necessary and sufficient for stimulation of GEF
66 activity[5] (**Extended data Fig. 1)**. Hereafter we refer to phosphorylated Ric-8A(1-491) as
67 Ric-8A and Δ31NGαi1 as Gα.

68 To stabilize, and limit the dynamics of the Ric-8A:Gα complex for crystallographic
69 and cryo-EM experiments, we developed a panel of camelid nanobodies (Nb)[20] that
70 specifically recognize either Gαi1, Ric-8A or the complex of the two. We formed a series
71 of Ric-8A:Gαi1:Nb complexes that included from one to four Nbs from this panel. The
72 stability of the complexes towards cryogenic vitrification and consequently, the quality
73 and resolution of cryo-EM reconstructions derived from them, was improved in step with
74 the number of Nbs in the complex. We determined the cryo-EM structure of a complex of
75 Ric-8A:Gαi1 with three Nbs bound to Ric-8A and one bound to the helical domain of Gα.

Together, these nanobodies do not significantly affect Ric-8A-GEF activity (**Extended Data Fig. 2**). The structure was determined from 327,493 particles derived from 8,468 movie images, yielding a 3.9Å resolution reconstruction (**Fig. 1, Extended Data Figs. 3 and 4 and Table 1**).

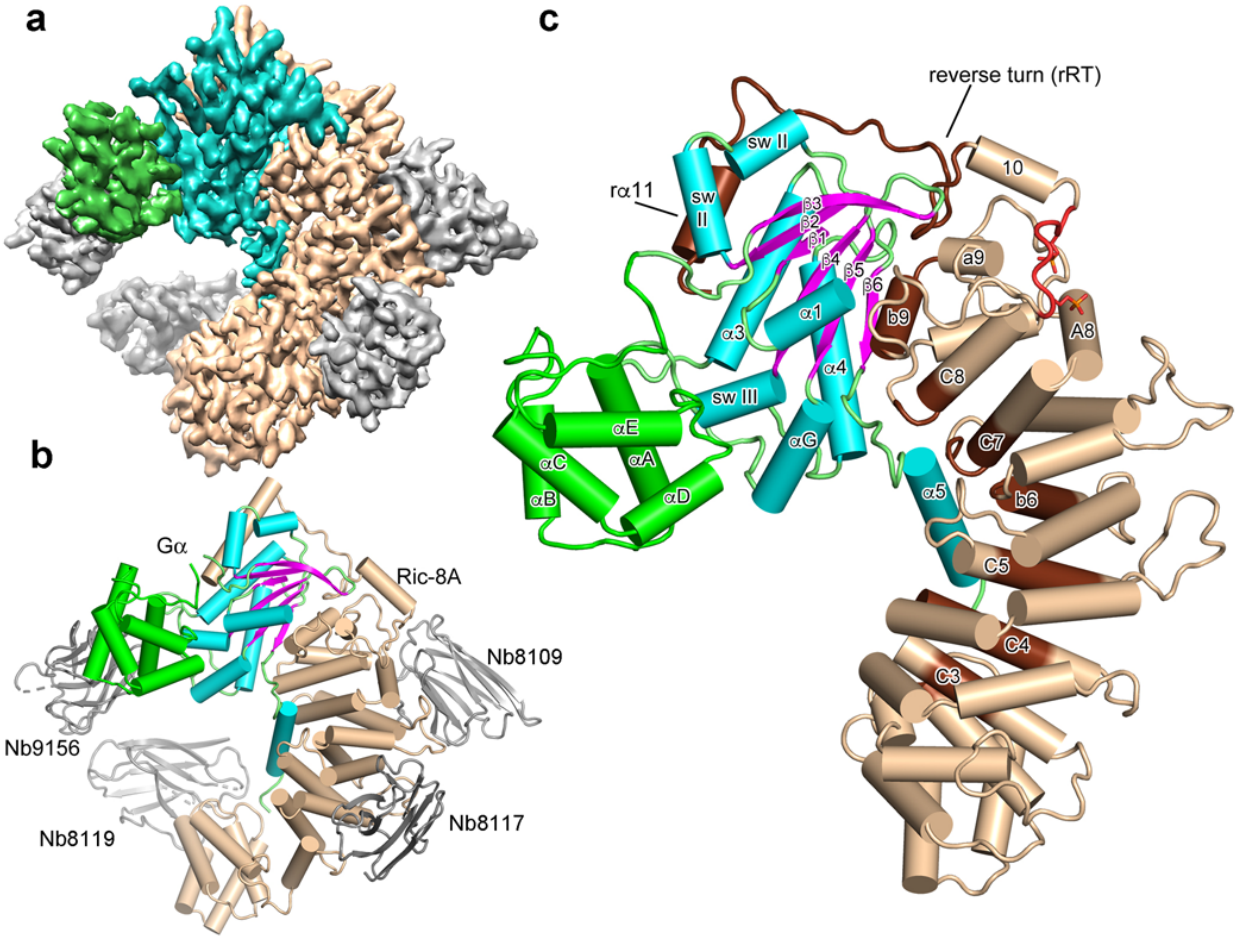

Figure 1. Architecture of the Ric-8A:Gα:4Nb complex. **a**, Cryo-EM 3D reconstruction of Ric-8A:Gα:4Nb is shown with Ric-8A colored *wheat*, Gα GTPase and Helical domains colored *cyan* and *green*, respectively, and nanobodies colored *gray*. **b**, Annotated ribbon and cylinder drawing, colored as in **a**, but with the β-strands of Gα rendered in *magenta*. (**C**) The Ric-8A:Gαi1:4Nb complex is shown with the nanobodies removed and the loop segments of the Gα GTPase domain colored green. Segments of Ric-8A that contact Gα are rendered in *dark brown*. Ric-8A residues 335-340, which include the two phosphorylation sites are rendered in *red*.

We obtained crystals of Ric-8A:Gαi1 bound to the three Ric-8A-specific Nbs used to generate the cryo-EM structure. Diffraction from these crystals was highly anisotropic (**Extended Data Fig. 5**), extending to 4.6Å along *a**, and *b**, and 3.3Å along *c**, affording

92 measurement of a 90% complete anisotropic dataset to 3.3Å resolution (**Extended Data**
93 **Table 2**). Initial crystallographic phases were determined by molecular replacement
94 and subsequently used to fit the cryo-EM density map. Iterative cycles of model-building
95 and refinement utilized both cryo-EM and X-ray diffraction data to generate the final
96 models **(Extended Data Table S1 and S2)**. In the following discussion, we use
97 prefixes "r" and "g" for residue and secondary structure identifiers of Ric-8A and Gα,
98 respectively. ARM/HEAT repeat helices of Ric-8A are designated according to their
99 position in the repeat: "A", "B" or "C" for ARM repeats or "a" and "b" for HEAT repeats,
100 followed by the sequence number of the repeat (1 through 9). We use the established
101 nomenclature for Gα secondary structure [21-23]. Descriptions of the crystal structure of
102 Ric-8A:Gα refer to chains A and B, the better ordered of the two complexes in the
103 asymmetric unit.
104 The cryo-EM reconstruction reveals Ric-8A residues 2-487 and the whole of Gα with
105 the exception of the disordered linker (residues 50-76) between the Helical and GTPase
106 domains (**Fig. 1a and 1b and Extended Data Video 1**). The crystal structure of the Ric-
107 8A:Gα complex also reveals continuous electron density for Ric-8A except for the
108 linkage between 422 and 430. Notably, residues C-terminal to the last HEAT repeat
109 (r430-r491) are disordered in structures of Ric-8A in which Gα is absent[4,18]. In the
110 crystal structure, which lacks Nb1056, the helical domain of Gαi1 and its connections to
111 the GTPase domain, including much of gα1 and all of switch I, are disordered.
112 Otherwise the cryo-EM and X-ray models of Ric-8A:Gα are in good agreement, although
113 certain irregularly-structured and loop regions in both Gα and Ric-8A show significant
114 divergence (**Extended Data Fig. 6**). Small angle X-ray scattering (SAXS)
115 measurements of the complex are consistent with the X-ray and cryo-EM structures
116 (**Extended Data Fig. 7**).

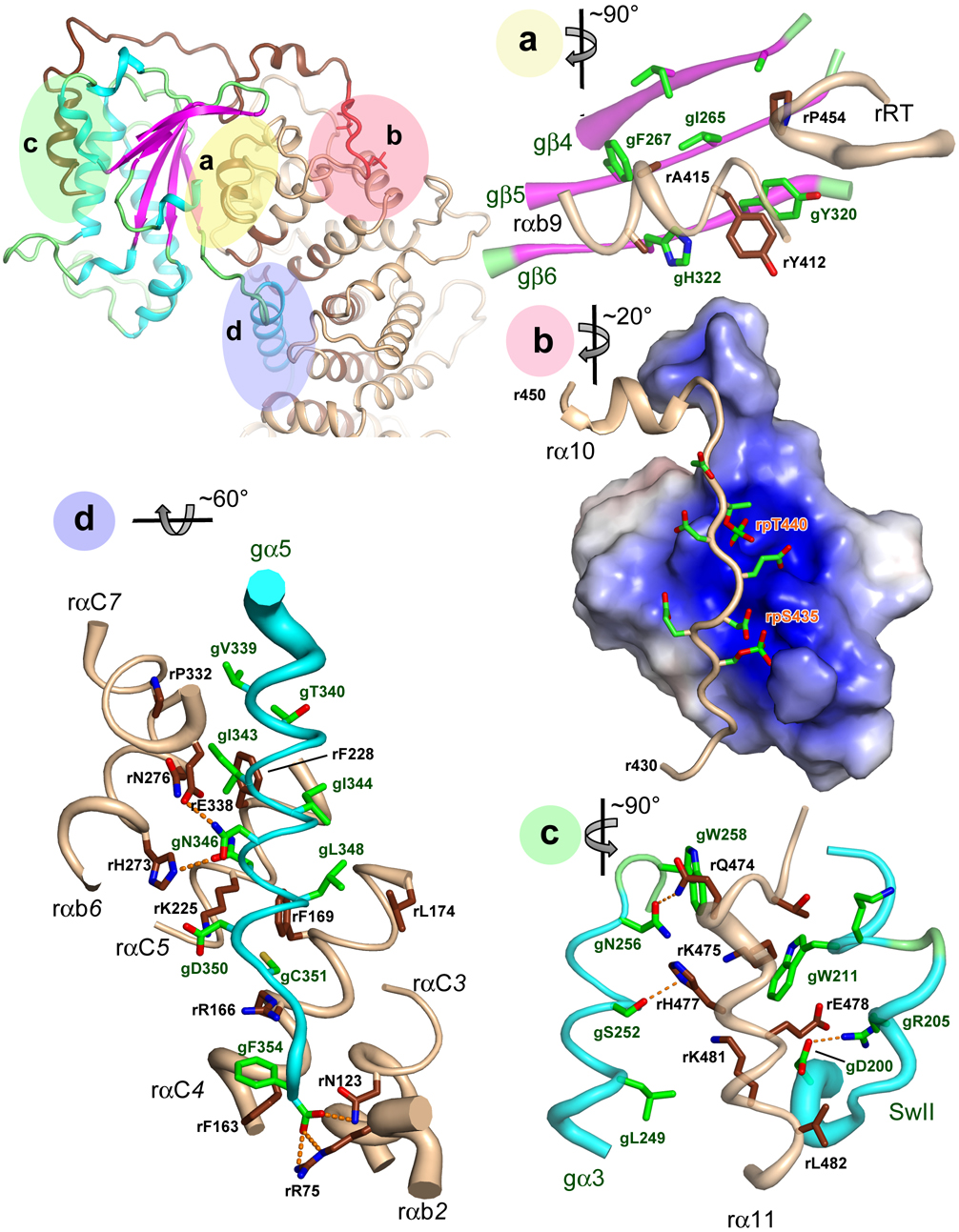

Figure 2. Interactions of Ric-8A with Gαi1. Three major Ric-8A:Gα contact surfaces and phosphorylation sites are highlighted and labeled in the *green*, *yellow*, *pink* and *blue* overlays (upper left) and enlarged in panels **a**-**d**. Axes adjacent to each panel label indicate the rotation applied to the overall schematic to generate the panel view. **a,** Interaction between Gα β-sheet and the Ric-8A C-terminal ARM/HEAT repeat helix rαA*9* and reverse turn r451-r457 (rRT) from the crystal structure. Polypeptide backbones are rendered as tubes, with diameter proportional to B-factor at Cα. Carbon atoms of Ric-8A and Gαi1 are rendered in *deep brown*, and green, respectively, and oxygen and nitrogen atoms are respectively colored *red* and *blue*. **b,** Acidic Ric-8A peptide with phosphorylated residues rpS335 and rpT440 bound to the positively charged surface formed by the 8th and 9th Ric-8A ARM/HEAT repeats from the crystal structure. **c,** Interaction of rα11 with gα3 and Switch II from cryo-EM. Putative hydrogen bonds (donor-acceptor contact < 3.5Å) are depicted with *orange* dashed lines. **d,** Contacts between gα5 and residues in successive ARM/HEAT repeats of Ric-8A, from the crystal structure.

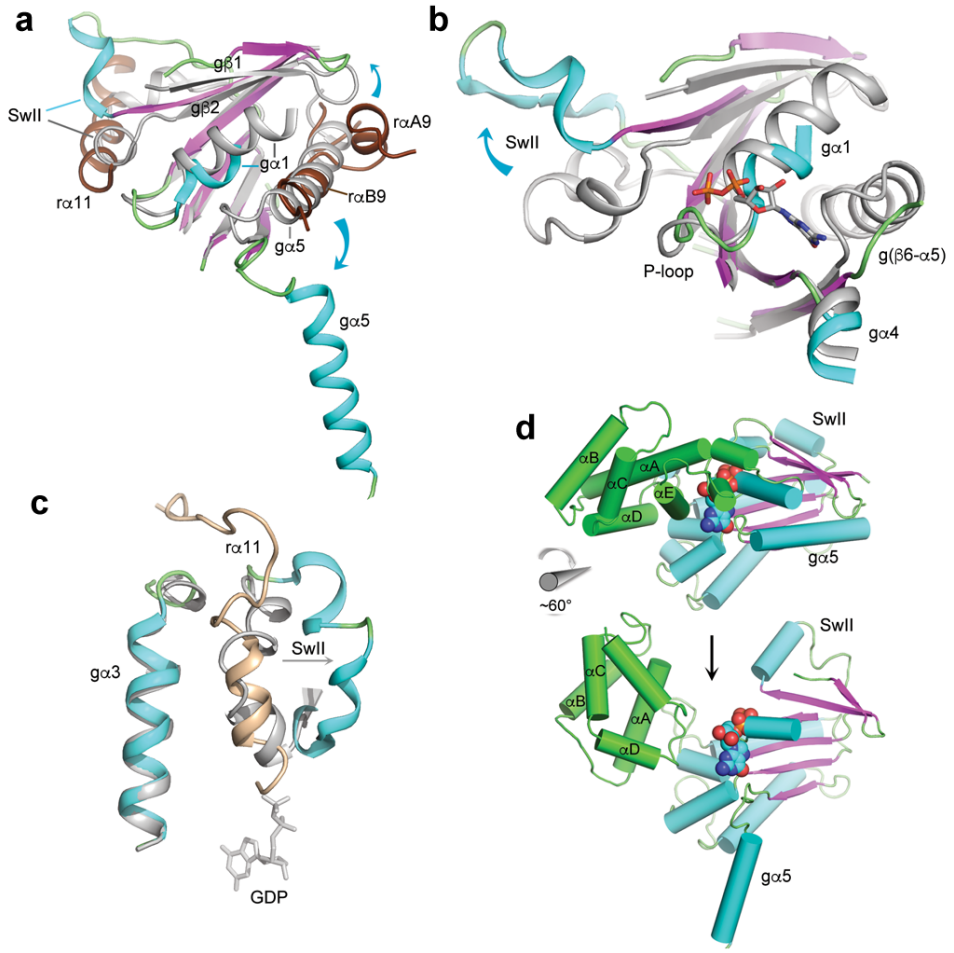

Figure 3. Conformational changes induced in Gα by its interaction with Ric-8A. In panels **a-c**, GDP•Pi-bound Gαi1 (PDB ID 1GIT), rendered in *gray* is superimposed on the crystal structure of Ric-8A-bound Gα using the Cα atoms of Gαi1 residues 219-225 (gβ4), 262-270 (gβ5) and 318-325. **a,** Conformational changes due to binding of Ric-8A αa9, αb9 and RT to Gαi1. **b,** Ric-8A-induced conformation changes dismantle the Gα nucleotide binding site (see text). GDP from 1GIT is included as a stick model for reference. **c**, Displacement of Switch II by r*α11*. The position of GDP bound to Gαi1•GDP is shown as a stick model. **d,** Ric-8A-induced rotation of the helical domain away from the GTPase domain of Gα: *top*, Gαi1•GDP (1GIT) rendered with helices as cylinders and β-strands as ribbons and the helical domain colored green; atoms of GDP are rendered as spheres. *Bottom*, the cryo-EM – derived model of Ric-8A-bound Gα with GDP from 1GIT shown as a reference point.

Binding of Ric-8A to the GTPase domain of Gα at three non-contiguous contact surfaces bury more than 3200Å^2 of solvent-accessible surface area (**Fig. 2a,c,d**). Together, these interactions destabilize the guanine nucleotide binding site (**Fig. 3**). At the core of the complex, Ric-8A αb9 (r401-r408) and the reverse turn r451-r457 (rRT) interact with the gβ4-gβ6 strands of Gα (**Fig. 2a and Extended Data Figs 8a and b**).

146 Ric-8 αb9 occupies the site of gα5 in GDP-bound Gα, and consequently gα5 is ejected
147 from the concave surface of the Gα β-sheet (**Fig. 3a**). Ric-8A residues rY412, rA415,
148 rA416 and rL418 in rαb9 substitute for nonpolar residues of gα5 to stabilize the
149 hydrophobic surface of the Gα β-sheet core. These residues are conserved in both A
150 and B isoforms of vertebrate Ric-8 (**Extended Data Fig. 9a**) and form Van der Waals
151 interactions with residues in gβ4-gβ6 that are conserved in both Gαi and Gαs families
152 (**Extended Data Fig. 9b**). The rW415A mutation severely impairs GEF activity (**Fig. 4**),
153 although the Y412A mutation does not. At the same interface, steric interactions with
154 rαa9 lever the antiparallel gβ2-gβ3 hairpin away from the GTPase core (**Fig. 3a**), thereby
155 destabilizing and partially disordering gα1. This, as described below, triggers separation
156 of the Helical and GTPase domains of Gα.

157 The ~90° rotation of α5 away from the GTPase domain core (**Fig. 3a**) reconfigures
158 the "TATC" motif in the g(β6-α5) GDP purine binding loop (**Fig. 3b)**. This structural
159 change perturbs the conserved NKKD motif (in gβ4-αG) that confers specificity for
160 guanosine nucleotides[24]. Displacement of these two loops dismantles the GDP purine
161 binding site. The hydrophobic contact between the N-terminus of gα4 and the Ric-8A
162 αB8-αC8 turn (**Extended Data Fig. 10)** is also important, as indicated by the impairment
163 of GEF activity resulting from the rL383E mutation (**Fig. 4**).

164 After its ejection from the Gα β–sheet, gα5 is accommodated in a broad trough
165 formed by helices rαb2 through rαB8 that line the concave surface of ARM/Heat
166 superhelix of Ric-8A (**Fig 2d and Extended Data Fig. 8g and h**), as observed also in
167 the structure of Ric-8A bound to the C-terminus of transducin[18]. The predominantly
168 hydrophobic amino acid residues of gα5 that interact with the Ric-8A trough (e.g. gF336,
169 gV339, gI343, gI344 and gL348) otherwise pack against the GTPase domain β-sheet of

170 nucleotide-bound Gα[25]. Most of the Ric-8A residues that contact gα5 are conserved in

171 Ric-8B **(Extended Data Fig. 9a**), whereas several of the Ric-8A-contacting residues in

172 gα5 are not conserved among Gα classes (**Extended Data Fig. 9b**).

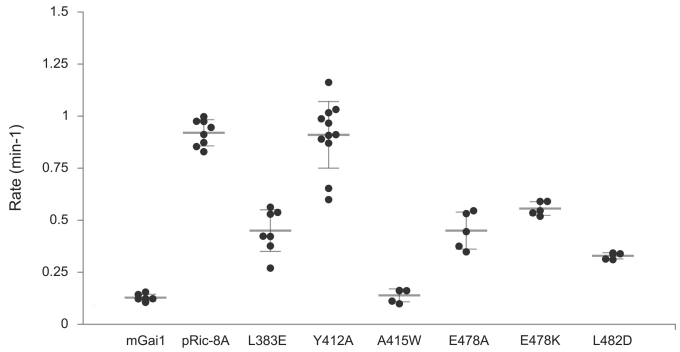

173 **Figure 4. Mutational analysis of selected residues at the Ric-8A:Gα interface**. GDP-GTP
174 exchange rates were measured by the rate of tryptophan fluorescence increase upon addition of ΔN31Gαi1
175 to Ric-8A and GTPγS at final concentrations of 2μM Ric-8A, 1μM ΔN31Gαi1 and 10μM GTPγS. Rate
176 differences between wild-type Ric-8A and all of the Ric-8A mutants with the exception of Y412A (P<0.82),
177 are significant at $10^{-5} > p > 10^{-12}$. Horizontal bars represent means and 1 standard deviation.
178

179 Ric-8A phosphorylation acts as an entropic clamp to promote GEF activity. The Ric-

180 8A αb9 and RT segments that interact with the Gα β-sheet are connected by an

181 intrinsically disordered sequence, r430-r450[4] followed by rα10. The segment from r430-

182 r440 is rich in acidic amino acids, and binds within a basic groove formed by rαA8 (r344-

183 r358) and rαa9 (r401-r410) (**Fig. 2b**). Phosphorylated rpS435 and rpT440, which are

184 well-ordered (**Extended Data Fig. 8i-l**) and form multiple ion-pair interactions with

185 conserved lysine and arginine side chains in the Ric-8A electropositive groove, help to

186 immobilize the r430-450 connector and consequently stabilize rαb9 and rRT that interact

187 with gβ4-gβ6. Accordingly, we found earlier that charge→neutral mutations of rR345Q

188 and rK349A, which interact with rpS435 and adjacent acidic residues, reduce both basal

189 and phosphorylation-stimulated GEF activity of Ric-8A[4].

190 Ric-8A helix α11 (r471-r491), which is preceded by an elongated peptide (r458-r470)

191 that forms an extended arch over the α3-β5 loop of Gα, packs between Gα Switch II

192 and gα3 (**Fig. 2c, and Extended Data Fig 8c-f**). In the GTP-bound state of Gα, these
193 two elements form the Gα effector protein binding site[26]. rα11 occupies the position of
194 Switch II in the G protein heterotrimer[27], and also in Gαi1 bound to GTP analogs[25] and in
195 the Gαi1•GDP•Pi product complex[28] (**Fig. 3c**). However, Switch II is disordered in
196 Gαi1•GDP and probably also in nucleotide-free Gα[22]. Ric-8A interactions with switch II
197 are functionally important, since mutations of two Gα-contacting residues in rα11, rE478
198 and L482, which are conserved in both Ric-8A isoforms, impair GEF activity (**Fig. 4**).
199 The conformations of Switch II observed in the X-ray and cryo-EM structures differ from
200 each other, and from those adopted in nucleotide-bound Gα[26] (**Extended Data Fig.**
201 **8e,f**). Remodeling of Switch II may be facilitated by Ric-8A-induced displacement of β2-
202 β3 (**Fig. 3a**) described above.

203 Displacement of gα5 and reorientation of gβ2-gβ3 eliminates a nexus of stabilizing
204 interactions with the C-terminal residues of gα1, which become disordered (**Fig 3a.**). As
205 a consequence, contacts between the GTPase and helical domains of Gα are disrupted.
206 As observed in the cryo-EM structure, the helical domain undergoes a clockwise rotation
207 of ~60° around an axis roughly aligned with αD of the Gα helical domain (**Fig. 3d**). By
208 this motion, a channel opens between the helical and GTPase domains, providing a path
209 of egress for the nucleotide. The magnitude of the rotation is less than that observed in
210 crystal and cryo-EM structures of GPCR:G protein complexes[16,29], or deduced from
211 double electron-electron resonance studies of Ric-8A:Gα[17], possibly because it is limited
212 by steric interactions between the nanobodies bound to Gα and Ric-8A. The variability in
213 the orientation of the helical domain is also suggested by normal-mode analysis of the
214 SAXS data (**Extended Data Fig. 7**). The coupled interactions between Ric-8A and Gαi1,

215 described above, induce profound conformational changes that dismantle the Gα
216 guanine nucleotide-binding site (**Fig. 3b and Extended Data Video 2**).

217 The basis for the Gα class selectivity of Ric-8 isoforms is not readily apparent.
218 The great majority of residues at the Gα contact residues are conserved in Ric-8A and
219 Ric-8B (**Extended Data Fig 9a**). Gα residues that interact with rαB9 and rRT are
220 conserved in the Gαi and Gαs classes. However, several residues in gα5 differ between
221 Gαs and Gαi classes (**Extended Data Fig. 9b**), and, as suggested[18], the latter may
222 engage in more productive interactions with Ric-8A than their Gαs counterparts.

223 The structure of the complex suggests elements of Ric-8A chaperone activity by
224 which it promotes folding and stabilization of nucleotide-free Gα[2]. It is remarkable that
225 the magnitude of conformational changes induced in Gαi1 by Ric-8A far exceed those
226 sufficient to effect GDP release in GPCR - G protein complexes[16,23] wherein gα5
227 undergoes a modest rotation and translation and switch II remains protected by Gβγ as
228 in the intact heterotrimer[27,30]. Rather, Ric-8A stabilizes nucleotide-free Gα subunits in
229 the absence of Gβγ[14]. Molecular dynamics simulations suggest that contacts between
230 gα5 and the Gα β-sheet are dynamic in nucleotide-free Gα[31]. Interactions with Ric-8A
231 would shield these hydrophobic surfaces from exposure in the cytosol. Switch II is also
232 a dynamic structure, even in the GDP-bound state of Gα[24] and would likewise be
233 stabilized by Ric-8A α11. Ric-8A(1-491) partially rescues Gαi1 biosynthesis in Ric-8A $^{-/-}$
234 cells, but not that of Gαq, for which full-length Ric-8A is required[32]. Hence, the C-
235 terminal ~40 residues of Ric-8A, which harbor three of the five CKII phosphorylation
236 sites[5], must play a critical role in Ric-8A chaperone activity. Nevertheless, it is clear that
237 the mechanism by which Ric-8A stabilizes dynamic regions of the nucleotide-free Gα
238 GTPase domain also underlie its GEF activity.

239 The extensive interface between Ric-8A and Gα prompts the question how the two
240 proteins are able to dissociate upon binding of GTP to Gα, a process that is kinetically
241 facile in comparison to the overall exchange reaction (**Fig. 5a and Extended Data Fig.**
242 **2**). Although displaced slightly by steric conflict with rα11 (**Fig. 3b**), the conformation of
243 the P-loop is largely retained in the nucleotide-free Gα bound to Ric-8A (**Fig. 5b**), thus
244 providing a preformed platform for subsequent binding of GTP. Electrostatic repulsion
245 between the C-terminus of r11 and the γ-phosphate of GTP as modeled in **Fig. 5b**, could
246 promote its release from its binding site between gα3 and Switch II, allowing Switch II to
247 refold into its native GTP-bound conformation. Disruption of Switch II interactions with
248 Ric-8A would restore the native structure of gβ2-gβ3, promote its interaction with gα1
249 and thereby destabilize the remaining interface of Ric-8A with the GTPase domain. The
250 dynamics that accompany Ric-8A binding to Gα•GDP and subsequent release of
251 Gα•GTP remain to be explored.

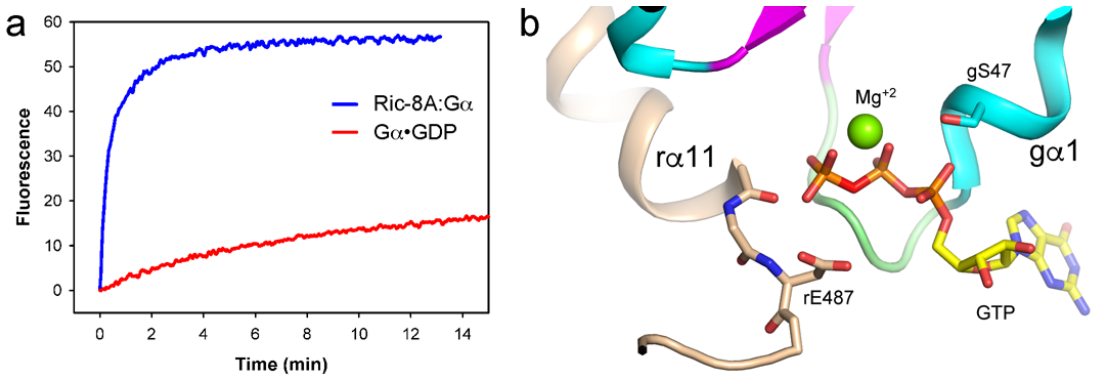

252

253 **Figure 5. The P-loop of Gαi1 provides a pre-ordered binding site for GTP in the complex with Ric-**
254 **8A. a**, Progress curve for GTP (10μM) binding to purified Ric-8A:Gαi1 complex (1μM) (*red*), relative to that
255 for nucleotide exchange at Gαi1•GDP (1μM). **b**, Superposition of a model of GTP (PDB ID 1CIP) onto the
256 nucleotide binding site of Ric-8A-bound Gαi1. Serine 47 of α1 is positioned for Mg^{+2} coordination (see text).

257 **References**

258

259 1 Tall, G. G., Krumins, A. M. & Gilman, A. G. Mammalian Ric-8A (synembryn) is a

260 heterotrimeric Galpha protein guanine nucleotide exchange factor. *J Biol Chem*

261 **278**, 8356-8362 (2003).

262 2 Chan, P., Thomas, C. J., Sprang, S. R. & Tall, G. G. Molecular chaperoning function

263 of Ric-8 is to fold nascent heterotrimeric G protein alpha subunits. *Proc Natl*

264 *Acad Sci U S A* **110**, 3794-3799, doi:10.1073/pnas.1220943110 (2013).

265 3 Gabay, M. *et al.* Ric-8 proteins are molecular chaperones that direct nascent G

266 protein alpha subunit membrane association. *Sci Signal* **4**, ra79, doi:4/200/ra79

267 [pii]

268 10.1126/scisignal.2002223 (2011).

269 4 Zeng, B. *et al.* Structure, Function, and Dynamics of the Galpha Binding Domain

270 of Ric-8A. *Structure*, doi:10.1016/j.str.2019.04.013 (2019).

271 5 Papasergi-Scott, M. M. *et al.* Dual phosphorylation of Ric-8A enhances its ability

272 to mediate G protein alpha subunit folding and to stimulate guanine nucleotide

273 exchange. *Sci Signal* **11**, doi:10.1126/scisignal.aap8113 (2018).

274 6 Miller, K. G. & Rand, J. B. A role for RIC-8 (Synembryn) and GOA-1 (G(o)alpha) in

275 regulating a subset of centrosome movements during early embryogenesis in

276 Caenorhabditis elegans. *Genetics* **156**, 1649-1660 (2000).

277 7 Couwenbergs, C., Spilker, A. C. & Gotta, M. Control of embryonic spindle
278 positioning and Galpha activity by C. elegans RIC-8. *Curr Biol* **14**, 1871-1876,
279 doi:S0960982204007456 [pii]10.1016/j.cub.2004.09.059 (2004).
280 8 Afshar, K. *et al.* RIC-8 Is Required for GPR-1/2-Dependent Galpha Function during
281 Asymmetric Division of C. elegans Embryos. *Cell* **119**, 219-230 (2004).
282 9 Woodard, G. E. *et al.* Ric-8A and Gi alpha recruit LGN, NuMA, and dynein to the
283 cell cortex to help orient the mitotic spindle. *Mol Cell Biol* **30**, 3519-3530,
284 doi:MCB.00394-10 [pii]10.1128/MCB.00394-10 (2010).
285 10 Tonissoo, T. *et al.* Nucleotide exchange factor RIC-8 is indispensable in
286 mammalian early development. *Dev Dyn* **239**, 3404-3415,
287 doi:10.1002/dvdy.22480 (2010).
288 11 Chan, P., Gabay, M., Wright, F. A. & Tall, G. G. Ric-8B is a GTP-dependent G
289 protein alphas guanine nucleotide exchange factor. *J Biol Chem* **286**, 19932-
290 19942, doi:M110.163675 [pii]10.1074/jbc.M110.163675 (2011).
291 12 Hinrichs, M. V., Torrejon, M., Montecino, M. & Olate, J. Ric-8: different cellular
292 roles for a heterotrimeric G-protein GEF. *J Cell Biochem* **113**, 2797-2805,
293 doi:10.1002/jcb.24162 (2012).
294 13 Papasergi, M. M., Patel, B. R. & Tall, G. G. The G protein alpha chaperone Ric-8 as
295 a potential therapeutic target. *Mol Pharmacol* **87**, 52-63,
296 doi:10.1124/mol.114.094664 (2015).

297 14 Thomas, C. J. *et al.* The nucleotide exchange factor Ric-8A is a chaperone for the
298 conformationally dynamic nucleotide-free state of Galphai1. *PLoS One* **6**, e23197,
299 doi:10.1371/journal.pone.0023197PONE-D-11-08669 [pii] (2011).
300 15 Kant, R., Zeng, B., Thomas, C. J., Bothner, B. & Sprang, S. R. Ric-8A, a G protein
301 chaperone with nucleotide exchange activity induces long-range secondary
302 structure changes in Galpha. *Elife* **5**, doi:10.7554/eLife.19238 (2016).
303 16 Rasmussen, S. G. *et al.* Crystal structure of the beta2 adrenergic receptor-Gs
304 protein complex. *Nature* **477**, 549-555, doi:nature10361
305 [pii]10.1038/nature10361 (2011).
306 17 Van Eps, N., Thomas, C. J., Hubbell, W. L. & Sprang, S. R. The guanine nucleotide
307 exchange factor Ric-8A induces domain separation and Ras domain plasticity in
308 Galphai1. *Proceedings of the National Academy of Sciences of the United States*
309 *of America* **112**, 1404-1409, doi:10.1073/pnas.1423878112 (2015).
310 18 Srivastava, D., Gakhar, L. & Artemyev, N. O. Structural underpinnings of Ric8A
311 function as a G-protein alpha-subunit chaperone and guanine-nucleotide
312 exchange factor. *Nat Commun* **10**, 3084, doi:10.1038/s41467-019-11088-x
313 (2019).
314 19 Nagai, Y., Nishimura, A., Tago, K., Mizuno, N. & Itoh, H. Ric-8B stabilizes the alpha
315 subunit of stimulatory G protein by inhibiting its ubiquitination. *J Biol Chem* **285**,
316 11114-11120 (2010).
317 20 Pardon, E. *et al.* A general protocol for the generation of Nanobodies for
318 structural biology. *Nat Protoc* **9**, 674-693, doi:10.1038/nprot.2014.039 (2014).

319 21 Lambright, D. G., Noel, J. P., Hamm, H. E. & Sigler, P. B. Structural determinants
320 for activation of the alpha-subunit of a heterotrimeric G protein. *Nature* **369**,
321 621-628 (1994).
322 22 Mixon, M. B. *et al.* Tertiary and quaternary structural changes in Gi alpha 1
323 induced by GTP hydrolysis. *Science* **270**, 954-960 (1995).
324 23 Flock, T. *et al.* Universal allosteric mechanism for Galpha activation by GPCRs.
325 *Nature* **524**, 173-179, doi:10.1038/nature14663 (2015).
326 24 Sprang, S. R. G protein mechanisms: Insights from structural analysis. *Annu Rev*
327 *Biochem* **66**, 639-678 (1997).
328 25 Coleman, D. E. *et al.* Structures of active conformations of Gi alpha 1 and the
329 mechanism of GTP hydrolysis. *Science* **265**, 1405-1412 (1994).
330 26 Sprang, S. R., Chen, Z. & Du, X. Structural basis of effector regulation and signal
331 termination in heterotrimeric Galpha proteins. *Adv Protein Chem* **74**, 1-65
332 (2007).
333 27 Wall, M. A. *et al.* The structure of the G protein heterotrimer Gi alpha 1 beta 1
334 gamma 2. *Cell* **83**, 1047-1058 (1995).
335 28 Berghuis, A. M., Lee, E., Raw, A. S., Gilman, A. G. & Sprang, S. R. Structure of the
336 GDP-Pi complex of Gly203-->Ala G_{ia1}: a mimic of the ternary product complex of
337 G_a-catalyzed GTP hydrolysis. *Structure* **4**, 1277-1290 (1996).
338 29 Westfield, G. H. *et al.* Structural flexibility of the G alpha s alpha-helical domain
339 in the beta2-adrenoceptor Gs complex. *Proc Natl Acad Sci U S A* **108**, 16086-
340 16091, doi:10.1073/pnas.1113645108 (2011).

341 30 Lambright, D. G. *et al.* The 2.0Å crystal structure of a heterotrimeric G protein.
342 *Nature* **379**, 311-319 (1996).
343 31 Dror, R. O. *et al.* SIGNAL TRANSDUCTION. Structural basis for nucleotide
344 exchange in heterotrimeric G proteins. *Science* **348**, 1361-1365,
345 doi:10.1126/science.aaa5264 (2015).
346 32 Oner, S. S. *et al.* Regulation of the G-protein regulatory-Galphai signaling
347 complex by nonreceptor guanine nucleotide exchange factors. *J Biol Chem* **288**,
348 3003-3015, doi:10.1074/jbc.M112.418467 (2013).
349

350 **Methods**

351 **Preparation of crosslinked Ric-8A and Gαi1** Bis-sulphosuccinimidyl suberate
352 (BS3), Pierce-Thermo-Fisher Scientific) was dissolved in water to a concentration of 100
353 mM. K100 reagent (CovalX) is provided as a 2 mg/ml aqueous solution and contained a
354 proprietary mixture of inert carbon chain spacers (lengths between 8.8-13.2 Å),
355 separating 1-hydroxyl-7-azabenzotriozole groups. Ric-8A:Gαi1 complex, prepared as
356 described[1-3] was dialyzed into 20 mM phosphate buffer saline (PBS) pH 7.4, 1 mM DTT,
357 and final concentration adjusted to 20 mM in the same buffer. For each 100 ml of
358 complex, 20 ml of K100 (2mg/ml) and 25 ml of BS3 (100 mM) was added, incubated at
359 room temperature for 30 minutes and the reaction quenched by addition of 10 ml of 1 M
360 Tris pH 8.5. Samples were centrifuged at 14,000 rpm on a desk-top centrifuge for 10 min
361 at 4°C, to remove particulate matter, eluted though a tandem 5 ml HiTrap desalting
362 column (GE Healthcare) to remove excess cross-linking reagents. Proteins were eluted
363 in 20 mM PBS, concentrated to 0.3 mg/ml and 1 mM fresh DTT added as the final step.
364 Cross-linked samples were analyzed by Coomassie-stained SDS-PAGE and verified by

365 Western blotting using an anti-Ric-8A monoclonal antibody[4] and mouse Anti-Gαi1
366 monocolonal antibody (Enzo Lifesciences). The crosslinked preparation contained
367 cross-linked Ric-8A:Gαi1, free Gαi1 and Ric-8A in roughly equal proportion.
368 **Development of Camelid nanobodies** Llamas (*Lama glama*) were immunized with
369 the cross-linked Ric-8A:Gαi1 preparation. Peripheral blood lymphocytes were isolated
370 from the immunized animals for extraction of total RNA, generation of cDNA and PCR
371 amplification to isolate cDNAs encoding heavy chain variable domains (VHH) for
372 subcloning into the pCTCON2 vector for display on the cell surface of *Saccharomyces*
373 *cerevisiae* EBY100 cells, as described[5-7]. Cells expressing nanobodies that selectively
374 recognize Gαi1, Ric-8A or the crosslinked Ric-8A:Gαi1 were identified by three-color
375 FACS sorting on a FACS AriaIII (BD Biosciences), using Dylight 505 (Pierce, Thermo
376 Scientific)-conjugated Ric-8A, Dylight 488-conjugated Gαi1 and R-phycoerythrin goat
377 anti-mouse antibody (Lucron) to label nanobody-expressing clones. Three rounds of
378 selection were conducted using 10mM fluorescent proteins in 20 mM PBS pH 7.4,
379 100mM NaCl and 2mM DTT. Nanobody sequences from selected clones yielding
380 nanobodies that exclusively bind to Gαi1, to Ric-8A either free or bound to Gαi1, or
381 exclusively to the Ric-8A:Gαi1 complex were subcloned in a pMESy4 vector for
382 periplasmic expression in *E. coli* WK6 cells as described[8]. Nanobody sequences encode
383 a C-terminal hexahistidine affinity tag.
384 Of the set of 27 nanobodies discovered in screening that show strong expression,
385 twenty were capable of binding to either free Ric-8A or to Ric-8A in complex with Gαi1
386 but not to Gαi1, three bound exclusively to the Ric-8A:Gαi1 complex and three bound to
387 Gαi1 or its complex with Ric-8A but not to Ric-8A alone. From this set was identified a
388 set of four nanobodies capable of binding simultaneously to Ric-8A:Gαi1, as determined
389 by co-elution as a stable hexameric complex from a GE Healthcare HiLoad 16/600

390 Superdex 200pg column and validated by mass spectrometry on a MicroFlex MALDI-
391 ToF MS(Brucker Microflex). Of this set, Nb8109, Nb8117 and Nb8119 bind to Ric-8A
392 and the Ric-8A:Gαi1 complex and Nb9156 binds to Gαi1.

393 **Nanobody expression and purification** Nanobodies (Nb) 8109, 8117, 8119
394 and 9156 were encoded in pMESy4 vectors for periplasmic expression in WK6
395 *Escherichia coli* cells[7]. Briefly, overnight cultures were grown in 50 ml LB media
396 containing 100 µg/ml Ampicillin, 100 mM Glucose, and 1 mM $MgCl_2$ in shaker flasks at
397 190 rpm and 37 °C. After ~16 hours cells were pelleted at 4000 rpm (2200xg) for 10
398 minutes using a benchtop Sorvall Legend RT. Re-suspended pellets were added to 1 L
399 TB media containing 100 µg/ml Ampicillin, 5 mM glucose, and 1 mM $MgCl_2$ then
400 incubated at 190 rpm and 37 °C until achieving an OD_{600} of 0.7-1.0, at which point
401 temperature was lowered to 28 °C and growths were induced with 300 µM isopropyl β-
402 D-1-thiogalactopyranoside (IPTG). Approximately 16 hours post-induction, cells were
403 pelleted at 8000 rpm (12000xg) for 15 min in a Sorvall RC 6+ Centrifuge and cell pellets
404 were stored at – 80 °C. Pellets were re-suspended in 100 ml of TES buffer (0.2 M Tris
405 pH 8, 0.5 mM EDTA, 0.5 M sucrose) at 4 °C, vortexed and allowed to stir for a minimum
406 of 1 hour. Cells were then added dropwise to a 200 ml solution of TES/4 buffer (0.05 M
407 Tris pH 8, 0.125 mM EDTA, 0.125 M sucrose), then stirred for 1 hour at 4 °C. Lysate
408 was then spun down at 8000 rpm (12000xg) for 30 min and supernatant was loaded on
409 a gravity column with Ni-NTA agarose resin (Qiagen). Nanobody-bound resin was
410 washed with 20 column volumes of Wash 1 (0.05 M Tris pH 8, 1 M NaCl), 5 column
411 volumes of Wash 2 (0.05 M MES pH 6, 1 M NaCl), 10 column volumes of Wash 3 (0.05
412 M Tris pH 8, 0.5 M NaCl), and then eluted with 3 column volumes of Elution Buffer (0.05
413 M Tris pH 8, 0.2 M NaCl, 0.5 M imidazole). Eluted nanobody was dialyzed overnight in
414 0.05 M Tris pH 8 and 0.2 M NaCl, then concentrated to 5-10 mg/mL before use or
415 storage at -80 °C. Before use all nanobodies were gel purified using a Superdex 200

416 10/300 GL size-exclusion column (GE Healthcare) in gel filtration buffer: 50 mM HEPES
417 pH 8, 150 mM NaCl, and 1 mM TCEP.
418 Complexes of Ric-8A, ΔN31Gαi1 and nanobodies Nb8109, Nb8117, Nb8119 in the
419 presence or absence of Nb9156 were formed by incubating Ric-8A, ΔN31Gαi1 and
420 nanobodies at a 1:2:2(per nanobody) molar ratio on ice for 16 hours and subsequently
421 purified by gel filtration chromatography using a GE Healthcare HiLoad 16/600 Superdex
422 200 pg in Gel Filtration Buffer.
423 **Gα and Ric-8A protein expression and purification** N-terminally glutathione-S-
424 transferase tagged Rat Gαi1 with a 31 residue N-terminal truncation (ΔN31Gαi1) was
425 expressed from a pDest15 vector in Bl21(DE3) RIPL *Escherichia coli* and purified as
426 previously described[1,9]. N-terminally hexahistidine tagged Rat Ric-8A(residues 1-491,
427 hereafter Ric-8A) was expressed and purified as previously described in a pET28a
428 vector with BL21(DE3) RIPL *Escherichia coli* cells[1,3,10]. Following removal of the
429 hexahistidine tag using Tobacco Etch Virus protease, Ric-8A protein was loaded onto a
430 Source 15Q column and eluted with a 500 mM NaCl gradient at 180 mM NaCl and
431 subsequently loaded on a GE Healthcare HiLoad 16/600 Superdex 200 column for size
432 exclusion chromatography in gel filtration buffer containing 50 mM Tris pH 8, 150 mM
433 NaCl and 1 mM Tris(2-carboxyethyl)phosphine (TCEP).
434 Ric-8A was phosphorylated using casein kinase II (New England Biolabs) as
435 previously described[10,11]. Briefly, purified Ric-8A was mixed 1:1 with a 2X Kinase
436 Reaction Buffer containing 0.1 M HEPES pH 8, 0.1 M NaCl, 20 mM $MgCl_2$, 2 mM EGTA,
437 and 1 mM DTT. ATP was added to a final concentration of 5 mM. 160 Units of casein
438 kinase II were added per mg of Ric-8A, and the reaction was allowed to proceed for ~16
439 hours at room temperature. Phosphorylated protein was loaded onto a Source 15Q
440 column pre-equilibrated with 50 mM HEPES pH 8, 25 mM NaCl, and 2 mM β-ME, and

441 eluted from a 500 mM NaCl gradient at 210 mM NaCl. Phosphorylated Ric-8A exhibits
442 an approximately 2 mS/cm shift compared to un-phosphorylated Ric-8A (**Extended Data**
443 **Fig. 1b**). All procedures described hereinafter were conducted with phosphorylated Ric-
444 8A comprising residues 1-491 of the full-length protein and referred to as Ric-8A.
445 Myristoylated Gαi1 (mGαi1), used in nucleotide exchange assays, was prepared as
446 described previously[10]. Mutants of Ric-8A, used in nucleotide exchange assays, were
447 constructed via the QuikChange II XL Site-Directed Mutagenesis Kit (Agilent).
448 Expression, purification and phosphorylation proceeded as described above.
449 **Guanine Nucleotide Exchange assays** were conducted by measuring the change
450 in Gαi1 tryptophan fluorescence in the presence or absence of Ric-8A using either
451 ΔN31Gαi1 or mGαi1, as described[3]. All proteins were buffer exchanged and assays
452 were conducted in 50 mM HEPES pH 8, 150 mM NaCl, 10 mM $MgCl_2$, 1 mM
453 TCEP. Experiments were carried out at 20°C using a LS55 luminescence spectrometer
454 (Perkin Elmer) with 4 nm slit widths (excitation 295 nm, emission 345 nm). GEF activity
455 for Ric-8A and Ric-8A mutants were measured by preincubating 450 µl of Ric-8A and
456 GTPγS in a quartz fluorescent cuvette prior to addition of 50 µl of 10 µM mGαi1 for a
457 final concentration of 0.5 µM Ric-8A, 1 µM mGαi1, and 10 µM guanosine 5'-O-[gamma-
458 thio]triphosphate (GTPγS) in 500 µl. GTPγS binding to size exclusion chromatography
459 purified complexes of Ric-8A: ΔN31Gαi1 with and without nanobodies were compared to
460 intrinsic nucleotide exchange of ΔN31Gαi1. GTPγS was added to preincubated
461 complexes for final concentrations of 1 µM complex (or ΔN31Gαi1) and 10 µM
462 GTPγS. For each assay, a minimum of 5 technical replicates were taken for each
463 sample; more replicates were performed if the series of assays was conducted over
464 several days, to control for changes in sample activity. Progress curves were fit to single
465 or double (If a slow binding phase was detected) exponential rate models using

466 SigmaPlot 7. Statistical significance of rate differences between reference and test
467 samples was determined by a two-tailed Student's t-test. Probability that differences are
468 derived from a random distribution is reported. All data points are shown in box plots
469 that show mean and standard deviation for each data set[12].

470 **Crystallization of the ΔN31Gαi1:Ric-8A:3Nb complex** Crystallization trials for the
471 Ric-8A:ΔN31Gαi1:Nb8109:Nb8117:Nb8119 complex were conducted by vapor diffusion
472 using commercially-available crystallization screening kits. Sitting drops were set on 96-
473 2 well INTELLI-PLATEs (Art Robbins Instruments) using a Gryphon crystallization robot
474 (Art Robbins Instruments) at 3-10 mg/mL protein complex at a 1:1 v/v ratio with
475 precipitation solution. Initial crystallization conditions were identified from hits on the
476 ShotGun screen (MD1-88 Molecular Dimensions). Further optimization was carried out
477 by grid screening variations in sodium malonate (Hampton Research) concentration and
478 pH and by crystal seeding by hanging drop on 24 well VDXm plates (Hampton
479 Research). Crystal seed stocks were prepared with the Seed Bead kit (Hampton
480 Research) in 1.4 M sodium malonate pH 6.9. 0.9 µl of protein stock was added to 0.6 µl
481 of reservoir and 0.3 µl of crystal seed stock and incubated at 12 °C for a minimum of 1-2
482 weeks. Optimal crystals were obtained from hanging drops containing 3.6 mg/ml Ric-
483 8A:ΔN31Gαi1:3Nb, 1.4 M sodium malonate pH 6.9 at 12 °C.

484 **Crystallographic data collection and processing** Diffraction data were measured
485 at the NSLS-II FXS beamline from LN_2 cryoprotected crystals measuring approximately
486 50µ X 50µ X 5µ employing a helical data collection mode[13], using X-rays of 0.9793
487 wavelength. A Si (111) double crystal monochromator was used to focus the X-ray
488 beam to a spot size of 1µ X 1µ at the sample. Data were measured in the Phi axis
489 rotation mode in 0.2° fames, at 0.06s/frame at a beam attenuation of 0.7. Diffraction
490 data were measured on an Eiger 16M detector at a 133 Hz frame rate. Due to

491 significant (> 0.5Å) differences in unit cell axis dimension between crystals, data from a
492 single crystal were selected for data processing and structure determination. In view of
493 the considerable anisotropy of diffraction (approximately 4.6Å along *a** and *b** and 3.3Å
494 along *c**), three separate data processing strategies were conducted using the
495 AutoPROC v1.0.2 software toolbox[14] for evaluation in subsequent model-building and
496 refinement steps. All three utilized XDS[15] for data indexing and initial integration. The
497 Standard Isotropic protocol uses SCALEA and TRUNCATE from the CCP4[16] to generate
498 isotropic data with a resolution cutoff (4.6Å) determined by the criteria $R_{pim} \geq 0.6$, $I/\sigma(I) \geq$
499 2.0 and $CC_{1/2} \geq 0.3$. The Extended Isotropic protocol employed POINTLESS and
500 AIMLESS scaling and analysis software[17] to generate scaled intensities extending to the
501 3.2Å resolution with $I/\sigma(I) \geq 1.2$. The Anisotropic Filtering protocol implemented in
502 STARANISO[18] generated a dataset that incorporates intensities within a locally
503 averaged value of $I/\sigma(I)$ to define an anisotropic diffraction cut-off surface (**Extended**
504 **data Table 2)**.
505 **Crystallographic model building and refinement** All crystallographic calculations
506 were conducted using the PHENIX 1.1.6 software package[19] unless otherwise noted.
507 Initial crystallographic phases for the Ric-8A:ΔN31Gαi1:3NB complex were determined
508 by Molecular Replacement using atomic coordinates of Ric-8A (residues 1-426; PDB
509 ID:6NMG), the Ras domain of Gai1:GDP (PDB ID: 1BOF), and an anti-VGLUT
510 nanobody (PDB ID:5OCL) as search models. An initial atomic model, consisting of
511 coordinates for Ric-8A residues 1-426, residues 34-65 and 190-320 of ΔN31Gαi1 and
512 three nanobody backbone models were manually refit into a sigma-weighted 2mFo-DFc
513 map using Coot v0.8.6[20] and refined using phenix.refine. Completion and refinement of
514 the crystallographic model followed the following general strategy: 1) model-fitting to the
515 cryo-EM reconstruction in regions of the structure in which the path of the polypeptide

516 chain was not defined in (or differed substantially from) the 2mFo-DFc map followed by
517 real space refinement with secondary structure and geometry restraints using
518 phenix.real_space_refine[21]; 2) refitting of the latter to the 2mFo-DFc map and
519 subsequent refinement; 3) refinement of the cryo-EM map (see below) using the
520 crystallographic model as an alignment reference. In the regions in which the
521 polypeptide path observed in the cryo-EM-derived and crystallographic models diverged,
522 no attempt was made to bring them into agreement. Initial cycles of crystallographic
523 model building and refinement were carried out using Standard Isotropic or Extended
524 isotropic data sets derived from datasets derived from merging and scaling data from the
525 two most strongly diffracting crystals. The final rounds of fitting and refinement of the
526 complete model (excluding the C-terminus of Gα1, the Helical Domain, and Switch I,
527 residues 51-184) utilized an Anisotropic Extended dataset comprising data from the
528 single crystal that afforded the strongest diffraction and optimal merging statistics (see
529 **Extended Data Table 2**). A TLS model was applied during refinement using
530 phenix.refine. Model quality and correlation with the refined electron density were
531 performed using MolProbity[22]. The atomic coordinates for the refined crystallographic
532 model for the Ric-8A:ΔN31Gαi1:3Nb complex and associated structure factors are
533 deposited in the RCSB Protein Data Bank[23] (PDB ID 6TYL). Figures depicting atomic
534 models were rendered using PyMol version 2.3 (Schrodinger, LLC)
535 **Cryo-EM data collection** Three microliters of the Ric-8A:ΔN31Gαi1:4Nb complex at
536 0.4 mg/ml with 0.01% NP40 were applied onto glow-discharged 200-mesh R2/1
537 Quantifoil grids (Electron Microscopy Sciences). Grids were blotted for 4 s and rapidly
538 cryocooled in liquid ethane using a Vitrobot Mark IV (Thermo Fisher Scientific) at room
539 temperature and 100% humidity. The samples were screened using a Talos Arctica
540 cryo-electron microscope (Thermo Fisher Scientific) operated at 200 kV and then

541 imaged in a Titan Krios cryo-electron microscope (Thermo Fisher Scientific) with GIF
542 energy filter (Gatan) at a magnification of 130,000× (corresponding to a calibrated
543 sampling of 1.06 Å per pixel). Micrographs were recorded using EPU software (Thermo
544 Fisher Scientific) with a Gatan K2 Summit direct electron detector, where each image is
545 composed of 30 individual frames with an exposure time of 6 s and a dose rate of 11.5
546 electrons per second per $Å^2$. A total of 8,670 movie stacks were collected with a defocus
547 range of -1.5 to -3.5 μm.

548 **Cryo-EM image processing** All micrographs were motion-corrected using
549 MotionCor2[24] and the contrast transfer function (CTF) was determined using
550 CTFFIND4[25]. All particles were autopicked using the NeuralNet option in EMAN2 v 2.31
551 and further checked manually, yielding 768,736 particles from selected 8,468
552 micrographs. Particle coordinates were then imported to Relion v3.0.6[4], wherein multiple
553 rounds of 2D classification were performed to remove poor 2D class averages.
554 Meanwhile, ~ 20,000 particle images were selected to build an initial model using the
555 "ab-initio 3D" program in cryoSPARC v2[26]. A total of 676,130 particles were used for 3D
556 classification in Relion to remove the no-conforming particles. Next, five rounds of 3D
557 heterogeneous refinement, CTF refinement were performed in cryoSPARC to further
558 remove the poor 3D classes. The final 3D refinement with 327,493 particles was
559 performed in cryoSPARC using the "non-Uniform refinement" option with a soft mask of
560 the complex density and a 3.85Å resolution map was obtained. The resolution of the
561 final map was estimated according to the 0.143 FSC criterion. A 3.9Å low-pass filter was
562 to the final 3D map for better display (See more information in **Extended Data Fig. 2**
563 **and Table I**).

564 **Cryo-EM model building** The cryo-EM model for the Ric-8A:ΔN31Gαi1:4Nbs
565 complex was constructed with a refined crystallographic Ric-8A:ΔN31Gαi:3Nb model (in

566 which only the GTPase domain was modeled) and a model of the helical domain of Gαi1
567 in complex with Nb9156 from the crystal structure of Gαi:Nb9156 complex (unpublished
568 data). The final Ric-8A:ΔN31Gαi1:4Nb cryo-EM model was rebuilt after refinement of the
569 cryo-EM reconstruction using a Ric-8A:ΔN31Gαi1:4NB mask as described above, with
570 multiple rounds of manual refitting of the cryo-EM density map optimized refinement
571 using phenix.real_space_refine with secondary structure and geometry restraints[21].
572 Model quality was evaluated with MolProbity[22].

573 **Small Angle X-ray Scattering data collection, analysis and modeling**

574 SAXS was performed at BioCAT beamline 18ID at the Advanced Photon Source,
575 Chicago, with in-line size exclusion chromatography (SEC-SAXS) to separate sample
576 from aggregates and other contaminants. Protein sample (approximately ~5 mg/ml in
577 50mM HEPES, pH 8.0, 150mM NaCl and 1mM TCEP) was loaded onto a Superdex 200
578 Increase 10/300 GL column, which was run at 0.7 ml/min in an AKTA Pure FPLC (GE
579 Healthcare Life Sciences). After detection by an in-line UV monitor, the sample passed
580 through the SAXS flow cell, a 1.5mm ID quartz capillary with 10μm walls. Scattering
581 intensity was recorded using a Pilatus3 1M (Dectris) detector which was placed 3.67m
582 from the sample affording access to a range of momentum transfer (q) from 0.0065$Å^{-1}$
583 to 0.35$Å^{-1}$ [$q=4\pi\sin(\theta)/\lambda$]. Exposures of 0.5 s were acquired every 2 seconds during
584 elution. Data were reduced using BioXTAS RAW v1.6.0[27]. Buffer blanks were created
585 by averaging regions flanking the elution peak and subtracted from exposures selected
586 from the elution peak to create the I(q) vs q curves used for subsequent analyses. *Ab*
587 *initio* molecular envelopes were computed by the ATSAS v2.6.2 package[28] programs
588 DAMMIN[29]. Ten bead models were reconstructed in DAMMIF[30], which were aligned and
589 averaged in DAMAVER[31] (Volkov, 2003). The Molecular envelope was visualized, and
590 atomic models fit to molecular envelopes using Chimera v1.10.2[32]. The conformational

591 flexibility of Ric-8A:ΔN31Gαi1 was modeled by coarse-grained fitting with respect to
592 experimental SAXS data using SREFLEX program in the ATSAS software package[28].
593 Normal mode analysis was conducted with automatic determination of rigid body units.
594 The final disposition of rigid body units after application of normal mode projections was
595 determined by rigid body refinement with respect to the computed SAXS profile[33].
596 CRYSOL software from the ATSAS software package was used to model scattering
597 profiles from atomic coordinates.
598 **Amino acid sequence alignments** were conducted using Clustal Omega[34] *via* its
599 web-server (https://www.ebi.ac.uk/Tools/msa/clustalo/).
600
601
602 **Data Availability** Coordinates of Ric-8A:ΔN31Gαi1:4Nb model from cryo-EM are
603 deposited in the RCSB Protein Data Bank (PDB) with ID 6UKT. Coordinates of Ric-
604 8A:ΔN31Gαi1:3Nb model from crystal structure are deposited in the PDB with ID 6YTL.
605 The cryo-EM reconstruction is deposited in the Electron Microscopy Data Bank
606 (https://www.ebi.ac.uk/pdbe/emdb/) with id EMD20812. The small angle X-ray scattering
607 data for the Ric-8A:ΔN31Gαi1 complex is deposited in the Small Angle Scattering
608 Biological Database (SASBDB)[35] with accession code SASDG95.
609
610
611

612 **Acknowledgements**

613 This research was supported by NIH R01GM105993 (S.R.S); NIH P41GM103832,
614 R01GM079429, and S10OD021600 (W.C.); NSF 1738547 (T-C.M); NIH R01-
615 GM088242 (G.G.T.); resources of Instruct-ERIC, part of the European Strategy Forum
616 on Research infrastructures (ESFRI), the Research Foundation-Flanders (FWO) for their
617 support to Nanobody discovery, and the Strategic Research Program (SRP) of the Vrije
618 Universiteit Brussel (E.P. and J.S.). The Integrated Structural Biology Core at the
619 University of Montana Center for Biomolecular Structure and Dynamics is supported by
620 NIH COBRE award P20GM103546 (S.R.S.). We thank Drs. Wuxian Shi and Martin
621 Fuchs at the National Synchrotron Light Source II (NSLS II) for assistance with data
622 collection at the FMX (17-ID-2) beamline, supported by NIH grant P41GM111244 and
623 the Department of Energy (DOE), KP1605010. Z.D. is supported by the SSRL Structural
624 Molecular Biology Program by the DOE and by NIH grant P41GM103393. Small angle
625 X-ray scattering experiments were conducted at the Advanced Photon Source, operated
626 for the DOE Office of Science by Argonne National Laboratory under Contract No. DE-
627 AC02-06CH11357 with support of NIH grant P41 GM103622 and 1S10OD018090-01 for
628 purchase of the Pilatus 3 1M detector. We thank Dr. Baisen Zeng for assistance with
629 GEF assays and SPR quantitation of Nb-Ric-8A binding.

630 **Author Contributions**

631 L.J.M. prepared and crystallized the Ric-8A:Gαi1:3Nb complex, assisted with X-ray data
632 collection, conducted mutagenesis studies and analyzed kinetic data.

633 K.Z. carried out image acquisition and processing, generated and refined cryo-EM
634 reconstructions.

635 T-C.M. fit and refined atomic models to cryo-EM and crystallographic data and

636 conducted SAXS analysis.

637 J.J. prepared and screened samples for cryo-EM data collection,and assisted with data
638 analysis.

639 C. Y-H. Conducted crystallization experiments and assisted with protein preparations.

640 S.L. assisted with cryo-EM data collection and processing.

641 C.J.T. prepared samples for nanobody development and conducted initial nanobody
642 characterization.

643 T.I.Z. advised on with X-ray data collection and processing.

644 S.T. and A.W. generated nanobodies.

645 G.G.T. provided general consultation on project.

646 J.S. oversaw nanobody development.

647 W.C. oversaw cryo-EM studies.

648 S.R.S. designed project, provided overall supervision, and wrote the manuscript with
649 assistance from co-authors.

650 **Competing interests statement**

651 The authors state no conflicting interests.

652 **Supplementary Information**

653 Supplementary Information is available for this paper

654 **Correspondence**

655 Correspondence and requests for materials should be addressed to Stephen Sprang:
656 Stephen.sprang@umontana.edu

657

658 **Methods References**

659

660 1 Thomas, C. J. *et al.* The nucleotide exchange factor Ric-8A is a chaperone for
661 the conformationally dynamic nucleotide-free state of Galphai1. *PLoS One* **6**,
662 e23197, doi:10.1371/journal.pone.0023197
663 PONE-D-11-08669 [pii] (2011).
664 2 Van Eps, N., Thomas, C. J., Hubbell, W. L. & Sprang, S. R. The guanine
665 nucleotide exchange factor Ric-8A induces domain separation and Ras domain
666 plasticity in Galphai1. *Proceedings of the National Academy of Sciences of the*
667 *United States of America* **112**, 1404-1409, doi:10.1073/pnas.1423878112 (2015).
668 3 Kant, R., Zeng, B., Thomas, C. J., Bothner, B. & Sprang, S. R. Ric-8A, a G
669 protein chaperone with nucleotide exchange activity induces long-range
670 secondary structure changes in Galpha. *Elife* **5**, doi:10.7554/eLife.19238 (2016).
671 4 Chan, P., Thomas, C. J., Sprang, S. R. & Tall, G. G. Molecular chaperoning
672 function of Ric-8 is to fold nascent heterotrimeric G protein alpha subunits. *Proc*
673 *Natl Acad Sci U S A* **110**, 3794-3799, doi:10.1073/pnas.1220943110 (2013).
674 5 Chao, G. *et al.* Isolating and engineering human antibodies using yeast surface
675 display. *Nat Protoc* **1**, 755-768, doi:10.1038/nprot.2006.94 (2006).
676 6 Young, C. L., Britton, Z. T. & Robinson, A. S. Recombinant protein expression
677 and purification: a comprehensive review of affinity tags and microbial
678 applications. *Biotechnol J* **7**, 620-634, doi:10.1002/biot.201100155 (2012).
679 7 Pardon, E. *et al.* A general protocol for the generation of Nanobodies for
680 structural biology. *Nat Protoc* **9**, 674-693, doi:10.1038/nprot.2014.039 (2014).
681 8 Abskharon, R. N. *et al.* Probing the N-terminal beta-sheet conversion in the
682 crystal structure of the human prion protein bound to a nanobody. *J Am Chem*
683 *Soc* **136**, 937-944, doi:10.1021/ja407527p (2014).

684 9 Thomas, C. J., Tall, G. G., Adhikari, A. & Sprang, S. R. Ric-8A catalyzes guanine
685 nucleotide exchange on G alphai1 bound to the GPR/GoLoco exchange inhibitor
686 AGS3. *J Biol Chem* **283**, 23150-23160 (2008).
687 10 Zeng, B. *et al.* Structure, Function, and Dynamics of the Galpha Binding Domain
688 of Ric-8A. *Structure*, doi:10.1016/j.str.2019.04.013 (2019).
689 11 Yu, W., Yu, M., Papasergi-Scott, M. M. & Tall, G. G. Production of
690 Phosphorylated Ric-8A proteins using protein kinase CK2. *Protein Expr Purif*
691 **154**, 98-103, doi:10.1016/j.pep.2018.10.002 (2019).
692 12 Weissgerber, T. L. *et al.* Data visualization, bar naked: A free tool for creating
693 interactive graphics. *J Biol Chem* **292**, 20592-20598,
694 doi:10.1074/jbc.RA117.000147 (2017).
695 13 Polsinelli, I. *et al.* Comparison of helical scan and standard rotation methods in
696 single-crystal X-ray data collection strategies. *J Synchrotron Radiat* **24**, 42-52,
697 doi:10.1107/S1600577516018488 (2017).
698 14 Vonrhein, C. *et al.* Data processing and analysis with the autoPROC toolbox.
699 *Acta Crystallogr D Biol Crystallogr* **67**, 293-302,
700 doi:10.1107/S0907444911007773 (2011).
701 15 Kabsch, W. Xds. *Acta Crystallogr D Biol Crystallogr* **66**, 125-132,
702 doi:10.1107/S0907444909047337 (2010).
703 16 Collaborative Computational Project, N. The CCP4 suite: programs for protein
704 crystallography. *Acta Crystallographica* **D50**, 760-763 (1994).
705 17 Evans, P. R. & Murshudov, G. N. How good are my data and what is the
706 resolution? *Acta Crystallogr D Biol Crystallogr* **69**, 1204-1214,
707 doi:10.1107/S0907444913000061 (2013).
708 18 Tickle, I. J. *et al.* STARANISO. (2018).

19 Adams, P. D. *et al.* PHENIX: a comprehensive Python-based system for macromolecular structure solution. *Acta Crystallogr D Biol Crystallogr* **66**, 213-221, doi:10.1107/S0907444909052925 (2010).

20 Emsley, P., Lohkamp, B., Scott, W. G. & Cowtan, K. Features and development of Coot. *Acta Crystallogr D Biol Crystallogr* **66**, 486-501, doi:10.1107/S0907444910007493 (2010).

21 Afonine, P. V. *et al.* Real-space refinement in PHENIX for cryo-EM and crystallography. *Acta Crystallogr D Struct Biol* **74**, 531-544, doi:10.1107/S2059798318006551 (2018).

22 Williams, C. J. *et al.* MolProbity: More and better reference data for improved all-atom structure validation. *Protein Sci* **27**, 293-315, doi:10.1002/pro.3330 (2018).

23 Berman, H. M. *et al.* The Protein Data Bank. *Nucleic Acids Res* **28**, 235-242. (2000).

24 Zheng, S. Q. *et al.* MotionCor2: anisotropic correction of beam-induced motion for improved cryo-electron microscopy. *Nat Methods* **14**, 331-332, doi:10.1038/nmeth.4193 (2017).

25 Rohou, A. & Grigorieff, N. CTFFIND4: Fast and accurate defocus estimation from electron micrographs. *J Struct Biol* **192**, 216-221, doi:10.1016/j.jsb.2015.08.008 (2015).

26 Punjani, A., Rubinstein, J. L., Fleet, D. J. & Brubaker, M. A. cryoSPARC: algorithms for rapid unsupervised cryo-EM structure determination. *Nat Methods* **14**, 290-296, doi:10.1038/nmeth.4169 (2017).

27 Hopkins, J. B., Gillilan, R. E. & Skou, S. BioXTAS RAW: improvements to a free open-source program for small-angle X-ray scattering data reduction and analysis. *J Appl Crystallogr* **50**, 1545-1553, doi:10.1107/S1600576717011438 (2017).

28 Franke, D. *et al.* ATSAS 2.8: a comprehensive data analysis suite for small-angle scattering from macromolecular solutions. *J Appl Crystallogr* **50**, 1212-1225, doi:10.1107/S1600576717007786 (2017).

29 Svergun, D. I. Restoring low resolution structure of biological macromolecules from solution scattering using simulated annealing. *Biophys J* **76**, 2879-2886 (1999).

30 Franke, D. & Svergun, D. I. DAMMIF, a program for rapid ab-initio shape determination in small-angle scattering. *J Appl Crystallogr* **42**, 342-346, doi:10.1107/S0021889809000338 (2009).

31 Volkov, V. V. & Svergun, D. I. Uniqueness of ab initio shape determination in small-angle scattering. *J Appl Crystallogr* **36**, 860-864 (2003).

32 Pettersen, E. F. *et al.* UCSF Chimera--a visualization system for exploratory research and analysis. *J Comput Chem* **25**, 1605-1612, doi:10.1002/jcc.20084 (2004).

33 Panjkovich, A. & Svergun, D. I. Deciphering conformational transitions of proteins by small angle X-ray scattering and normal mode analysis. *Phys Chem Chem Phys* **18**, 5707-5719, doi:10.1039/c5cp04540a (2016).

34 Sievers, F. *et al.* Fast, scalable generation of high-quality protein multiple sequence alignments using Clustal Omega. *Mol Syst Biol* **7**, 539, doi:10.1038/msb.2011.75 (2011).

35 Valentini, E., Kikhney, A. G., Previtali, G., Jeffries, C. M. & Svergun, D. I. SASBDB, a repository for biological small-angle scattering data. *Nucleic Acids Res* **43**, D357-363, doi:10.1093/nar/gku1047 (2015).

Extended Data Table 1 Cryo-EM Data Collection and Refinement Statistics	
Data collection and processing	Ric-8A(491):Δ31NGαi1:4Nb
Microscope	Titan Krios
Voltage (kV)	300
Camera	Gatan K2 Summit
Pixel size (Å)	1.06
Total Dose (e-/Å^2)	69
Defocus range (μm)	-1.5 to -3.5
Number of micrographs	8,670
Number of initial particles	768,736
Symmetry	C1
Number of final particles	327,493
Resolution (0.143 FSC, Å)	3.90
Atomic model refinement	
Software	phenix.real_space_refine
Clashscore, all atoms	8.79
Poor rotamers (%)	0.57
Favored rotamers (%)	99.43
Ramachandran favored (%)	84.24
Ramachandran allowed (%)	15.76
MolProbity score	2.15
Bond RMSD (Å)	0.006
Angle RMSD (Å)	1.005

Extended Data Table 2
Crystallographic Data Collection and Refinement Statistics

Data collection	Ric-8A(491):Δ31NGαi1:3NB		
Software	AutoPROC/STARANISO	XDS/AIMLESS	SCALA
Reflection scaling method[#]	Anisotropic filtered (extended)	Isotropic (extended)	Isotropic (standard)
Wavelength (Å)	0.979	0.979	0.979
Resolution range (Å)*	39.58 - 3.3 (3.9 - 3.3) [a*, b*=4.6, c*=3.3]	39.65 - 3.3 (3.9 - 3.3)	39.65 - 4.6 (4.7 - 4.6)
Space group	$P\ 2_1$	$P\ 2_1$	$P\ 2_1$
Unit cell dimensions			
a, b, c (Å)	93.0 144.7 114.4	93.0 144.7 114.4	93.0 144.7 114.4
β (°)	94.7	94.7	94.7
Total reflections*	73843 (3449)	160159 (62218)	58730 (2930)
Unique reflections*	20707 (1035)	44840 (17203)	16296 (796)
Redundancy*	3.6 (3.3)	3.6 (3.6)	3.6 (3.7)
Completeness [spherical] (%)*	45.8 (6.0)	99.1 (99.1)	99.1 (99.5)
Completeness [ellipsoidal] (%)*	90.1 (58.2)	98.3 (91.5)	
Mean I/σ (I)*	3.7 (1.7)	1.9 (0.3)	4.1 (2.2)
Wilson B-factor	91.88		
R_{meas} †,*	0.21 (0.70)	0.55 (4.65)	0.18 (0.54)
$R_{p.i.m.}$ †,*	0.11 (0.38)	0.29 (2.42)	0.10 (0.28)
$CC_{1/2}$ †	0.99 (0.70)	0.97 (0.17)	0.99 (0.86)
Refinement			
R_{work} †,*	0.248 (0.319)		
R_{free} †,*	0.287 (0.323)		
CC_{work} †*	0.907 (0.719)		
CC_{free} †*	0.866 (0.893)		
Number of total atoms			
protein	15938		
total protein residues	2021		
RMS deviations			
bond lengths (Å)	0.002		
bond angles (◦)	0.55		
Ramachandran favored (%)††	89.16		
Ramachandran allowed (%)††	10.53		
Ramachandran outliers (%)††	0.30		
Rotomer outliers (%)††	0.0		
Clash Score††	10.32		
Average B-factor			
Macromolecules	109.97		
Number of TLS groups	1		

[#] The standard isotropic scaling method uses the classical isotropic treatment in truncate program where the resolution cut is determined by (1) Rpim ≤ 0.6. average I/σ(I) in a resolution bin ≥ 2.0, and $CC_{1/2}$ ≥ 0.3. The extended isotropic method includes all the measurements within the sphere of the highest observed resolution limit where the local [I/σ(I) ≥ 1.2; the extended anisotropic method uses the anisotropically-filtered reflections by STARANISO with the same resolution limit as the extended isotropic method. [*] Data for highest resolution shell are given in brackets. [†] $R_{meas}=\sum_{hkl}(n/n\text{-}1)^{1/2}\sum_i |I_i(hkl)-\langle I(hkl)\rangle|/\sum_{hkl}\sum_i I_i(hkl)$, where $I_i(hkl)$ is the *i*th observation of the intensity of the reflection *hkl* and $\langle I_{hkl}\rangle$ is the mean over *n* observations. $R_{p.i.m.}=\sum_{hkl}(1/n\text{-}1)^{1/2}\sum_i |I_i(hkl)-\langle I(hkl)\rangle|/\sum_{hkl}\sum_i I_i(hkl)$. [§] $R_{work}=\sum_{hkl}||F_{obs}|-|F_{calc}||/\sum_{hkl}|F_{obs}|$, where F_{obs} and F_{calc} are the observed and calculated structure-factor amplitudes for each reflection *hkl*. R_{free} was calculated for 5% of the diffraction data that were selected randomly and excluded from refinement. Correlation coefficients: $CC = S_i((x_i - \langle x\rangle)(y_i - \langle y\rangle))/(S_i((x_i - \langle x\rangle)^2(y_i - \langle y\rangle)^2)^{1/2}$, where x_i and y_i are the *i*th of *n* observations of quantities whose mean values are $\langle x\rangle$ and $\langle y\rangle$; for $CC_{1/2}$, x_i, and y_i correspond to intensity measurements derived from each of two randomly selected half-data sets from the set of unmerged data; For CC_{work} and CC_{free} x_i and y_i refer to observed structure factor amplitudes and structure factor amplitudes computed from the refined atomic model, respectively, for the working data set and the set used to compute R_{free}. [††]Calculated using MolProbity[39]

a

```
NB_8109  AQVQLQESGGGLEQAGDSLRLSCAASGLIVSNYAMGWFRQAPGKEREFVAYINWNGGVTY  60
NB_9156  -QVQLQESGGGLEQAGDSLRLSCAASGLIVSNYAMGWFRQAPGKEREFVAYINWNGGVTY  59
NB_8117  -QVQLQESGGGLVQPGGSLRLSCAASGIIFRSNGMAWYRQAPGKEREWVASITSFGDA-I  58
NB_8119  -QVQLQESGGGLVQAGGSLRLSCAASGGIVHISSMGWFRQAPGKQRELVATSPSNGDI-R  58
          *********** * *.********** *.   .*.*:******:** **     *.

NB_8109  YTNSVKGRFTISRDNAKNTVYLQMNSLKPEDTAVYYCARTSRASVTTRVADFGYWGQGTQ  120
NB_9156  YTNSVKGRFTISRDNAKNTVYLQMNSLKPEDTAVYYCARTSRASVTTRVADFGYWGQGTQ  119
NB_8117  YRDSVKGRFTISRDNARNAVSLQTNSLKTEDTAVYYCNTYPV---------NSAWGQGTQ  109
NB_8119  YADSVKGRFTLSRDNAKNTVSLQMNSLEPEDTAVYYCHSFLRHTAS--ASYNNYYGQGTQ  116
         * :*******:*****:*:* ** ***: ********               . :*****

NB_8109  VTVSSHHHHHHEPEA 135
NB_9156  VTVSSHHHHHHEPEA 134
NB_8117  VTVSSHHHHHHEPEA 124
NB_8119  VTVSSHHHHHHEPEA 131
         ***************
```

b

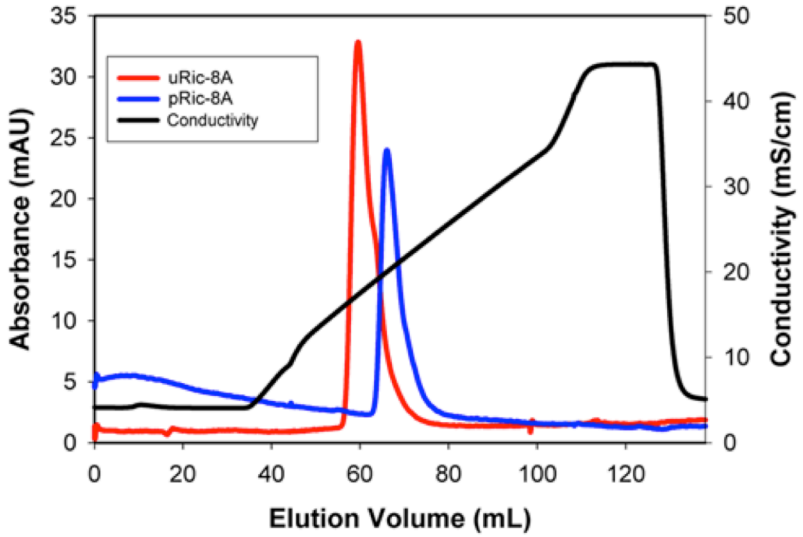

c

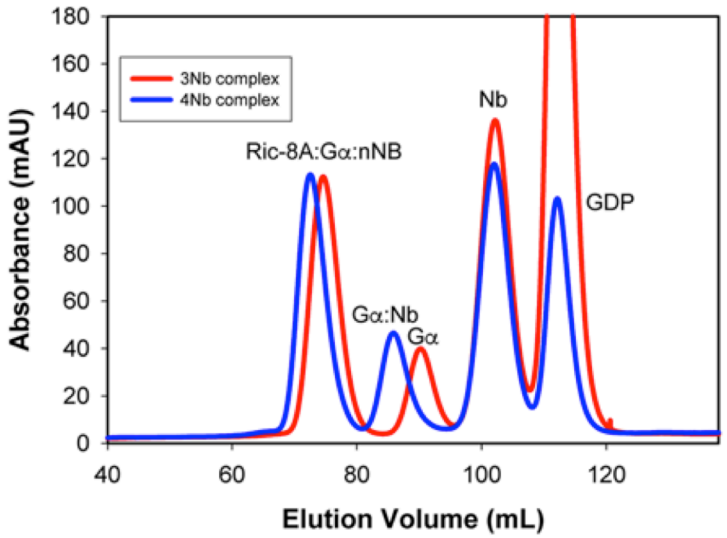

Extended Data Figure 1. Purification of Ric-8A:Gα:Nb complexes. **a**, Amino acid sequences of nanobodies used to form complexes. **b**, Anion exchange chromatography of phosphorylated (pRic-8A) and unphosphorylated (uRic-8A). **c**, Gel filtration of complexes at the following molar stoichiometric ratios: 1 Ric-8A:2 Gα:2 Nb 8109:2 Nb 8117:2 Nb 8119 (*red)* and 1 Ric-8A:2 Gα:2 Nb 8109:2 Nb 8117:2 Nb 8119:4 Nb 9156 (*blue*) molar stoichiometric ratios, Ric-8A and Ga correspond to the 1-491 residue construct of Ric-8A and the 31N-terminal truncation mutant of Gαi1, respectively, as described in the main text. (see Methods).

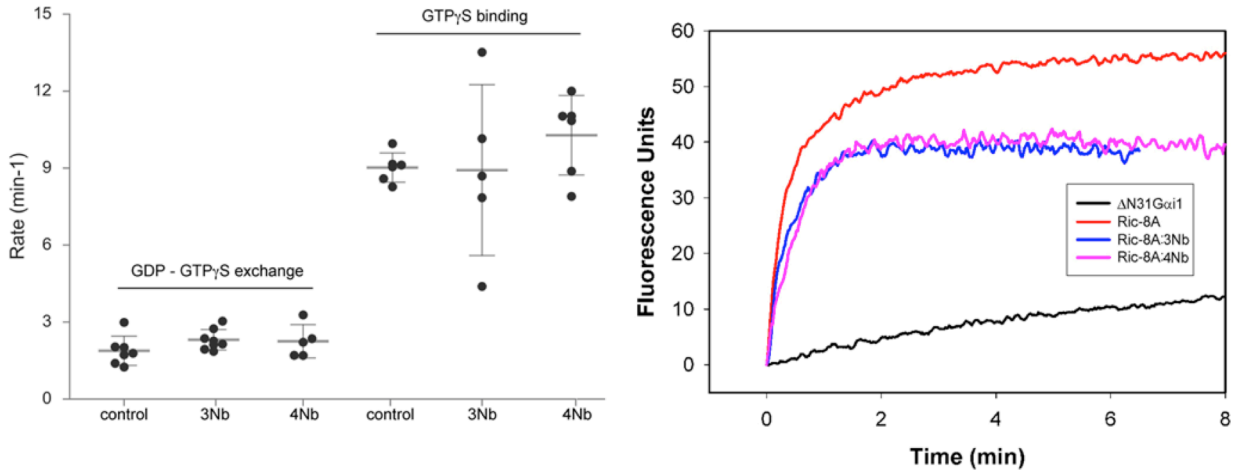

Extended Data Figure 2 Effect of nanobodies on GEF activity of Ric-8A. a, GDP-GTP exchange rates were measured by the rate of tryptophan fluorescence increase upon addition of ΔN31Gαi1 to Ric-8A and GTPγS at final concentrations of 2mM Ric-8A, 1mM ΔN31Gαi1 and 10mM GTPγS in the absence (control) or presence of Nb 8109 (4 mM), Nb 8117 (4 mM), Nb 8119 (4 mM) (3Nb) or the latter with the addition of (4 mM) Nb 9156 (4Nb). GTP binding rates were measured by tryptophan fluorescence increase upon addition of GTPγS (10 mM final concentration) to size exclusion chromatography-purified Ric-8A:ΔN31Gαi1:nNb (1 mM). Progress curves for the 3Nb and 4Nb GDP-GTPγS exchange and 4Nb GTPγS binding assays were fit to a single exponential rate, whereas data for controls and the 3Nb GTPγS binding assay were fit to a double exponential model, due to the presence of a slow kinetic phase, and the kinetic constant of the fast rate (k1) reported. In all cases average and standard deviations of measurement are reported for a minimum of 5 experimental replicates. **b**, Sample progress curves for the data reported in panel **a.**

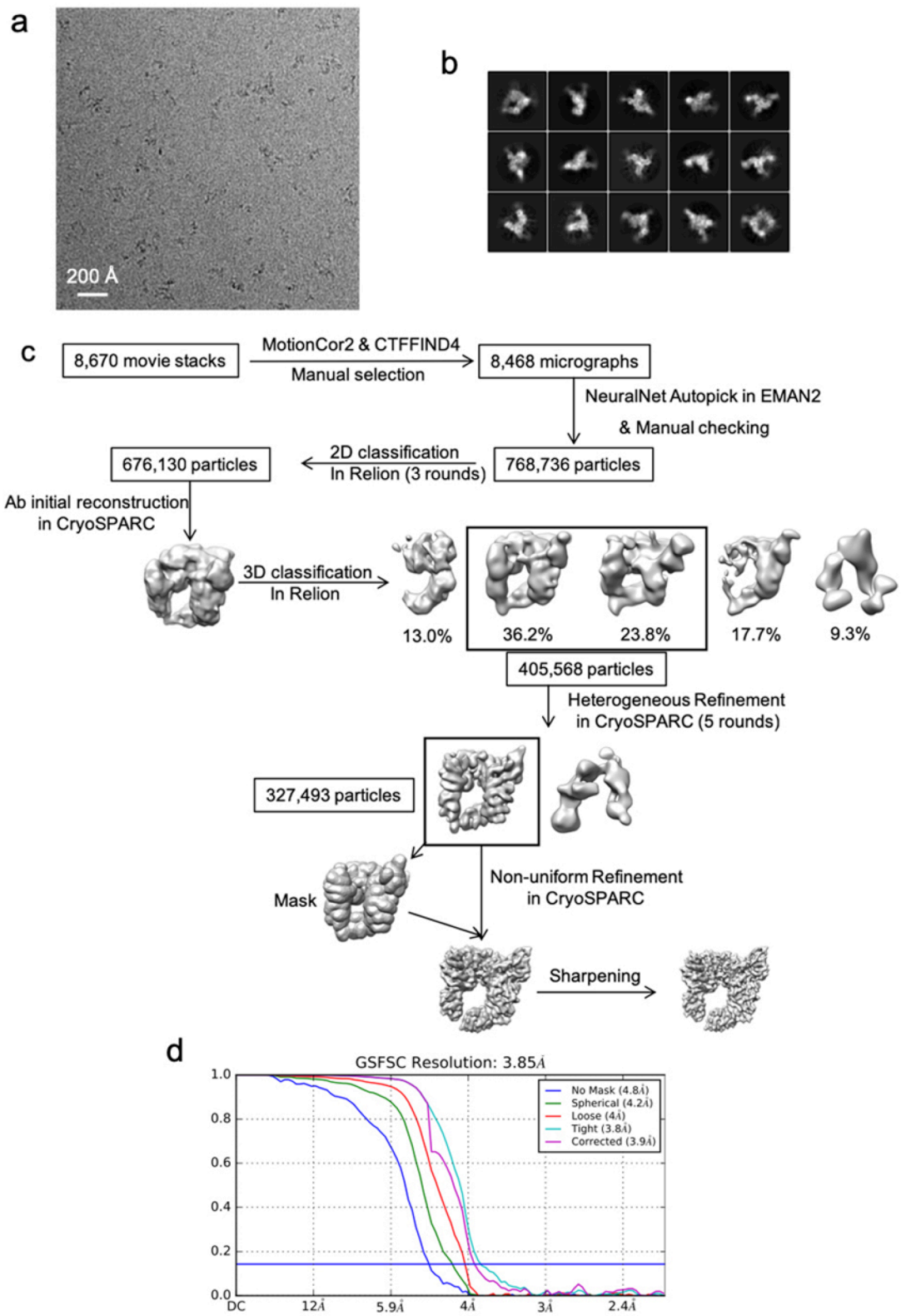

Extended Data Figure 3. Single-particle cryo-EM of Ric-8A:Ga:4Nb complex and Work-flow of cryo-EM image processing. a, Representative motion corrected cryo-EM micrograph. **b**, Reference-free 2D Class averages computed in Relion. **c**, Work-flow for cryo-EM processing (see Methods). **d**, Gold-standard Fourier Shell Correlation plot for 3D reconstruction generated using cryoSPARK.

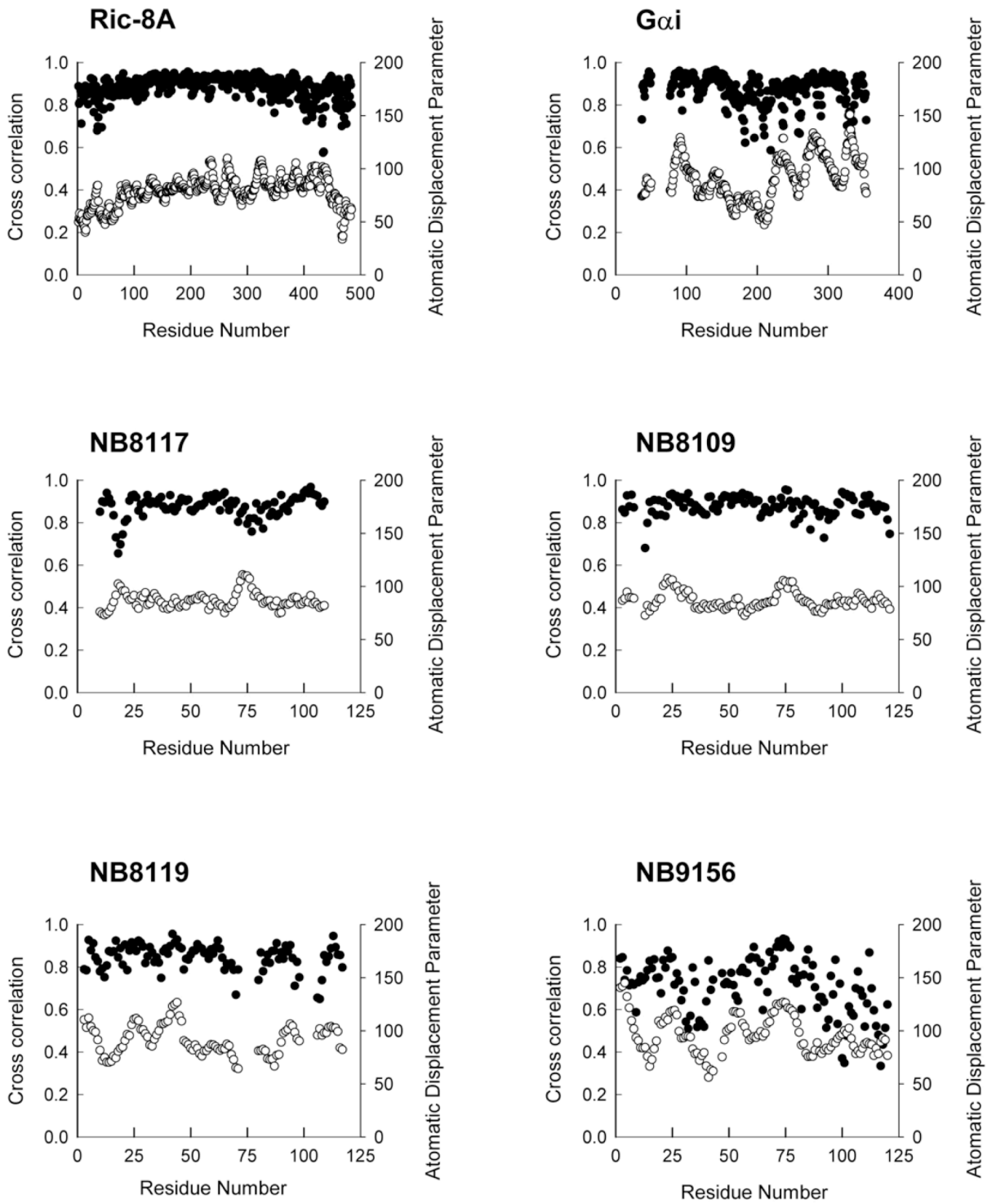

Extended Figure 4. Real-space refinement of Ric-8A:Gα :cryoEM model. Model-map correlation (filled circles) and B factors (open circles) are plotted with respect to residue number for the macromolecular components of the Ric-8A:Gα:4NB model derived from cryo-EM. Data were generated using the phenix.real_space_refine program from the PHENIX suite.

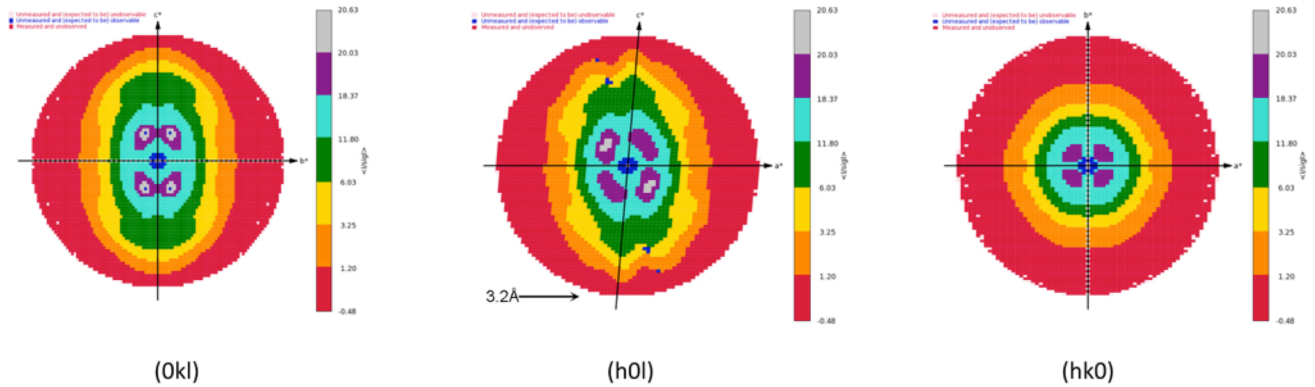

Extended Figure 5. Projections of diffraction intensities from crystals of the Ric-8A:Gα:3Nb complex along reciprocal cell axes and color-coded by I/σI. Data generated using the STARANISO sever (see Methods).

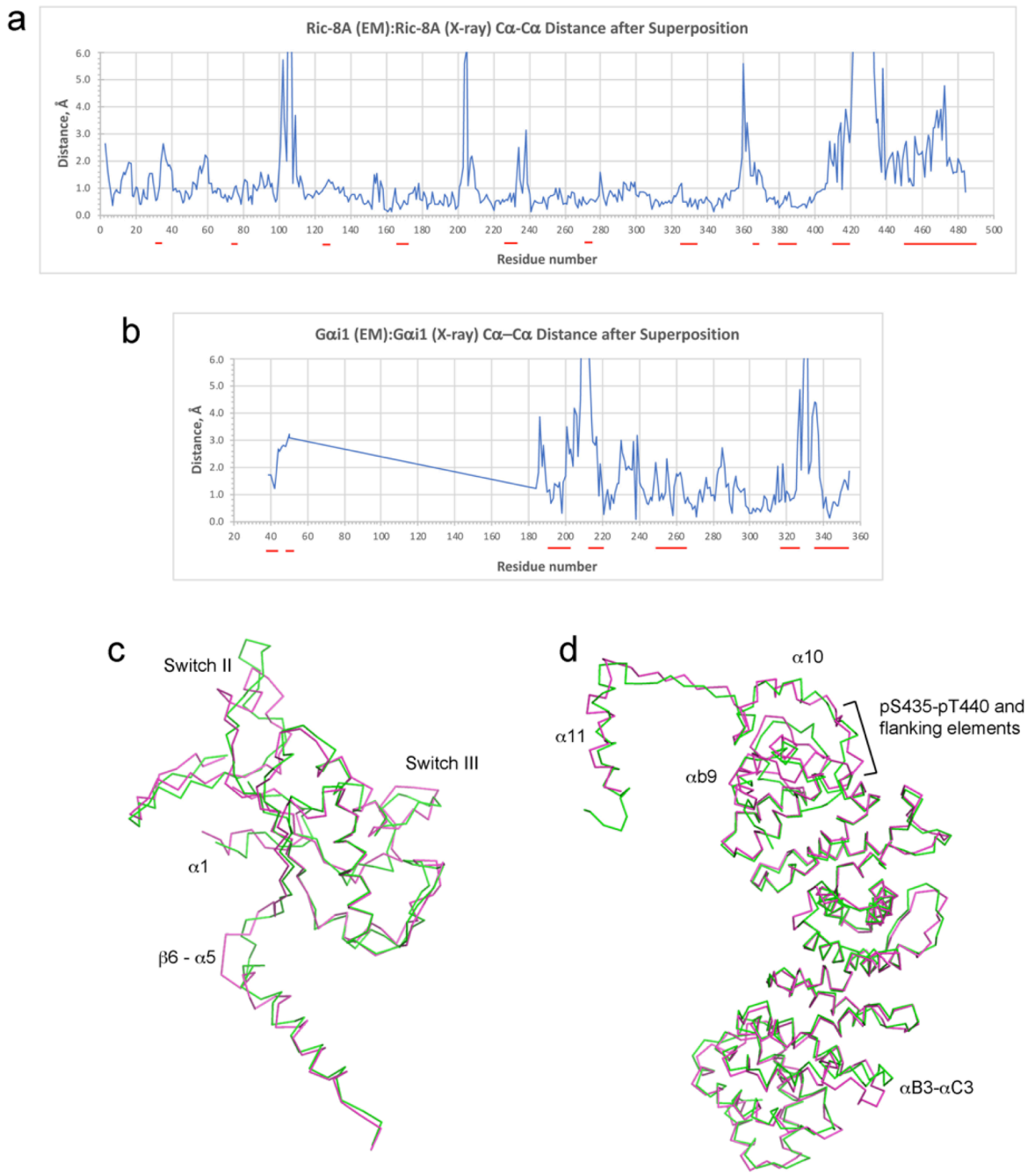

Extended Data Figure 6. Agreement of cryo-EM and X-ray structures of Ric-8A:Gαi1. a, Deviation between corresponding Cα atoms after least-squares superposition of Ric-8A coordinates. *Red* lines below residue numbers mark regions at which Ric-8A contacts Gai1 (see also ED Figure 10). The RMSD for all 484 common Cα positions is 1.81Å. The PyMOL align routine yields an RMSD of 1.03Å after rejection of 69 outliers. **b**, Deviation between Gαi1 atoms, computed per panel **a**. The RMSD for all 183 common Cα positions is 2.36Å; PyMol align yields an RMSD of 1.49Å after rejection of 21 outliers**. c,** Superposition of cryoEM (*magenta*) and X-ray (*green*) structures of Gαi1. Structural elements that show the largest structural differences are labeled. **d**, Superposition of Ric-8A models, as per panel **c.**

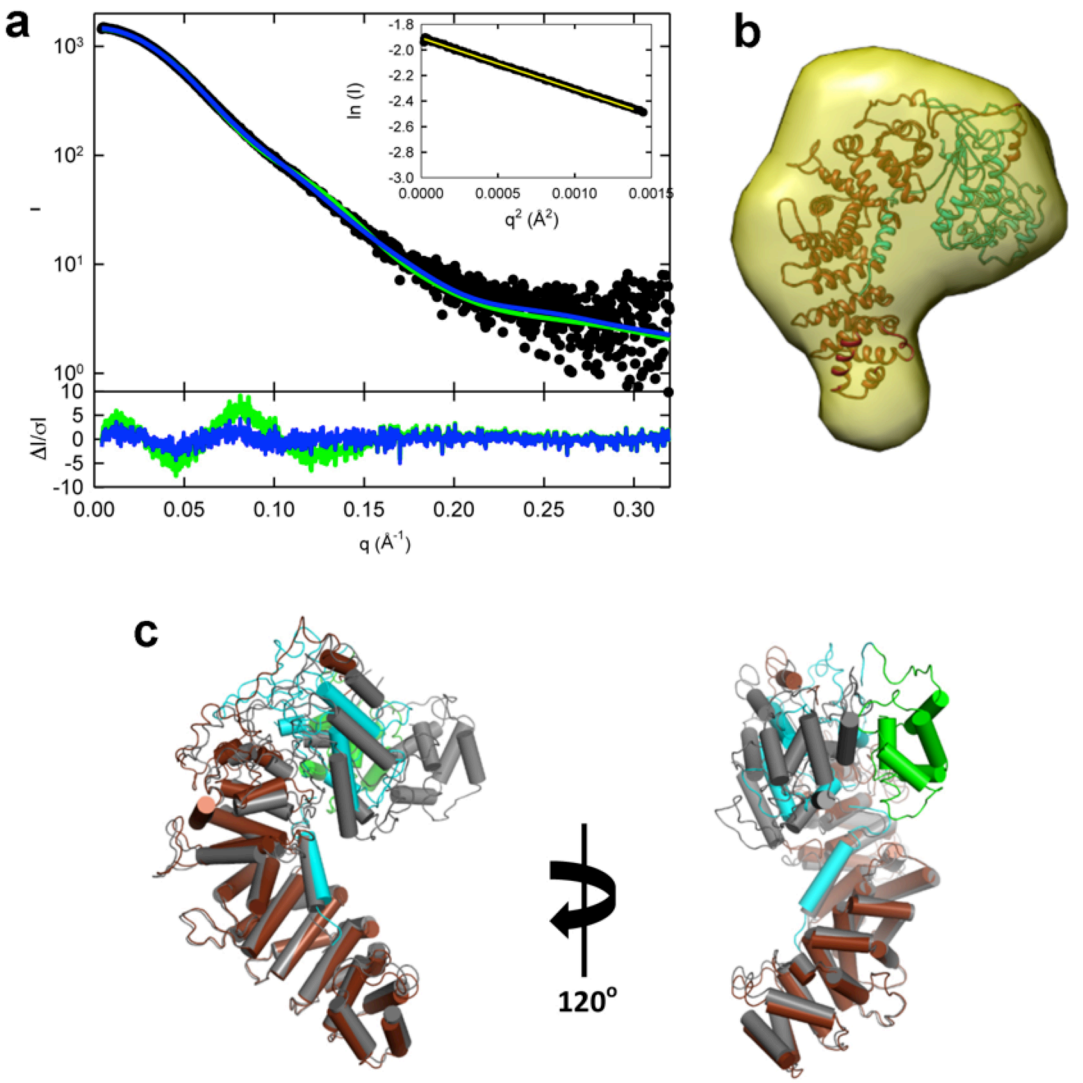

Extended Figure 7. Solution structure and Normal Mode refined model of Ric-8A:Δ31NGαi1 complex from Small-Angle X-ray scattering. **a**, Solution scattering profile for Ric-8A:ΔN31Gαi1 complex (*closed circles*). Inset shows, associate Guinier plot. CRYSOL and SRELEX from the ATSAS software package were used, respectively, to compute scattering profiles from atomic coordinates, and use normal-mode analysis to generate a refined atomic model. Computed scattering curves for cryo-EM-derived atomic coordinates of Ric-8A:ΔN31Gαi1 complex are shown in *green* and that from normal mode analysis is rendered in *blue*. The χ^2 for the fit of the computed scattering curve for the cryo-EM model is 5.48 and that for the normal-mode refined model is 1.24. The bottom panel shows the error-weighted residual difference plots $\Delta I/\sigma I = (I(q)_{experimental} - CI(q)_{model})/\sigma I(q)$ *vs q*, where C is a normalizing scale factor. **b,** SREFLEX-refined Ric-8A:ΔN31Gαi1 model fit to the *ab initio* molecular envelope calculated from the experimental SAXS scattering curve (*yellow*). **c**, Superposition of the SREFLEX-refined model of Ric-8A:ΔN31Gαi (Ric-8A, *brown*; GTPase domain of ΔN31GαI, *cyan*; Helical domain of ΔN31GαI, *green*) onto the cryo-EM model (*gray*), indicating a mode of helical domain rotation that may be preferred in solution in the absence of nanobodies. Models were superimposed using the Cα atomic positions of Ric-8A.

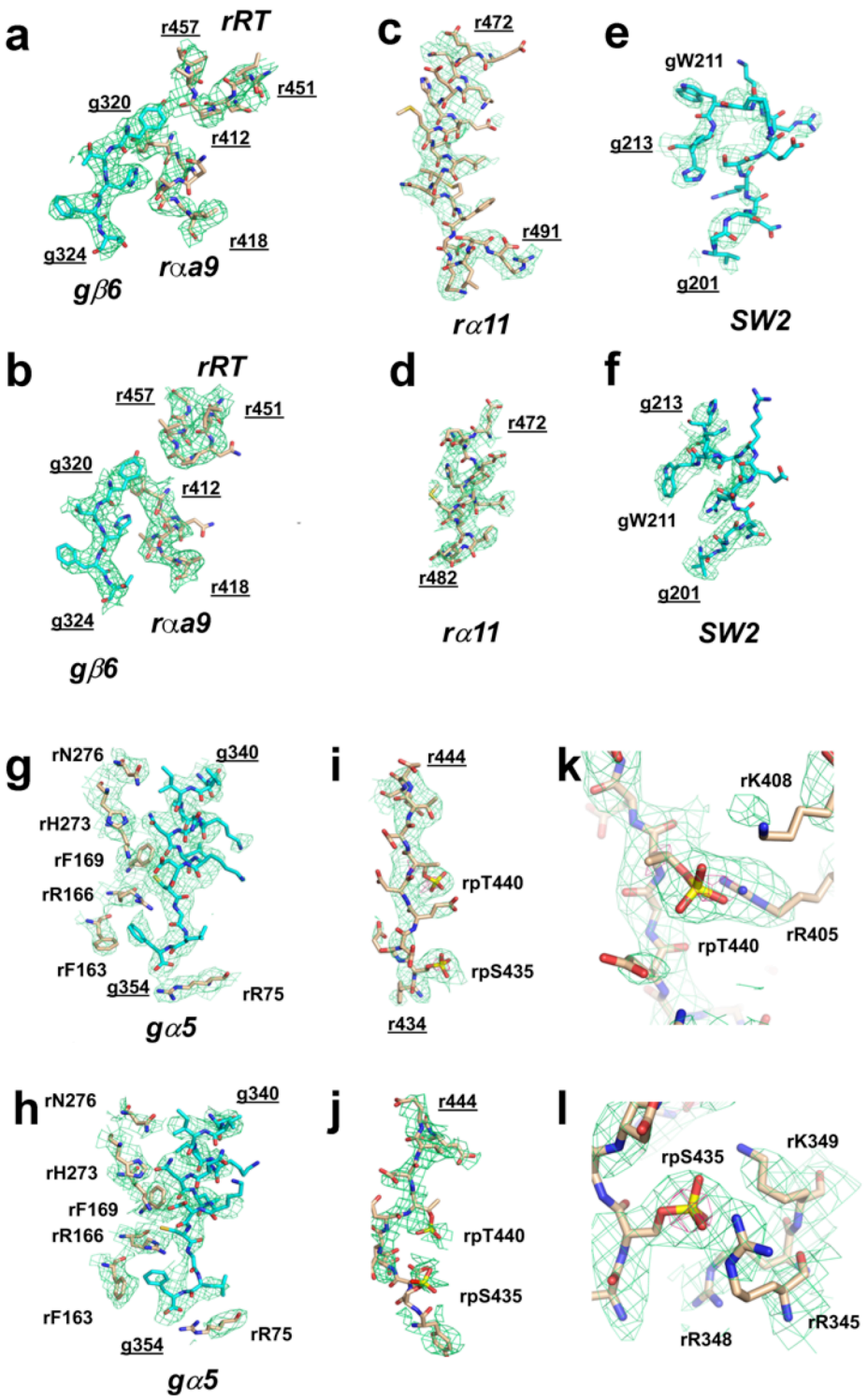

Extended Data Figure 8. X-ray and cryo-EM density at selected residue ranges. 2DFo-mFc electron density is contured at 1.0 σ and cryo-electron density is contoured at a threshold of 3.5. Structural elements of Ric-8A and Gαi1 are labeled in bold italics, N- and C-terminal residue numbers of segments are shown underlined, selected residues are labeled. Carbon atoms in Ric-8A are colored *wheat* and in Gai1, *cyan*. Panels **a, c, e, g** and **i** show residues from crystallographic model with corresponding density. Panels **b, d, f, h** and **j** show the same from the cryo-EM model. Panels **k** and **l**, show the crystallographic model and associated density around phospho-serine 435 and phospho-threonine 440, respectively. The 5 s contour level is shown in *red*.

```
Ric8A_RAT      28 EHSQSFTF 71 RILSRDRSCL 121 LCNLVLSSPTAQ 160 VQFFDLRLLFLLTAL
Ric8A_MOUSE    28 EHSQSFTF 71 RILSRDRSCL 121 LCNLVLSSPTAQ 160 VQFFDLRLLFLLTAL
Ric8A_HUMAN    28 EHSQSFTF 71 RILSRDRNCL 121 LCNLVLSSPVAQ 160 VQFFDLRLLFLLTAL
Ric8A_BOVIN    28 ENSQSFTF 71 RILSRDRSCL 121 LCNLVLSSPVAQ 160 VQFFDLRLLFLLTAL
Ric8A_DANRE    28 EKSQCFSF 71 RILSRDKKSL 121 LCNIVFNSEAAQ 160 VRFFDLRLTFLITAL
Ric8A_CHICK    28 EKSQCFTF 71 RILSRDKYCL 121 LCNIVFSSPRAQ 160 VKFFDLRLLFLLTAL
Ric8A_XENTR    28 ENSQCFFF 71 RILSRDKHAL 122 LCNIIYNSVEAQ 161 SKFFDLRLLFLLTAL
Ric8B_DANRE    28 ENSRTFAF 71 RILSRDKHVL 127 LCNVVFNSVPAQ 164 VGLFSLRLLFLLSAL
Ric8B_XENTR    16 QNRTMFKF 59 RILSRDKKVL 109 LCNIVFNSMEAQ 148 IRCFALRLLFLLTLL
Ric8B_CHICK    30 ENRAVFRF 73 RILSRDKKVL 123 LCNIIFNSAVAQ 162 IKCFDLRLLFLLSLL
Ric8B_HUMAN    38 KHRATFKF 71 RILSRDKKVL 121 LCNIVFNSQMAQ 160 IKCFDLRLLFLLSLL
Ric8B_BOVIN    28 KHRATFKF 71 RILSRDKKVL 121 LCNIVFNSQMAQ 160 IKCFDLRLLFVLSLL
Ric8B_MOUSE    28 KHRATFKF 71 RILSRDKKIL 121 LCNIVFNSQMAQ 160 IKCFDLRLLFVLSLL
Ric8B_RAT      28 KHRATFKF 71 RILSRDKKIL 121 LCNIVFNSQVAQ 160 IKCFDLRLLFVLSLL
                  ::  -* *    ******:  *     ***::-.*  **       -* *** *::: *
                     αb1        αb2            αC3            αC4

Ric8A_RAT     225 KVLFNITFDSV 267 TEEFHGHTVNLLG 320 LHQTHRLKECVAPVLSVLTE 361 DVRTRPEVGDLLR
Ric8A_MOUSE   225 KVLFNITFDSV 267 TEEFHGHTVNLLG 320 LHQTHRLKECVAPVLNVLTE 361 DVRTRPEVGDLLR
Ric8A_HUMAN   226 KVLFNITLDSI 268 TEEFHGHAVNLLG 321 LHKTHRLKESVAPVLSVLTE 362 DVRTRPEVGEMLR
Ric8A_BOVIN   225 KVLFNITFDSI 267 TEELHGHAVNLLG 320 LHQTHRLKESVAPVLSVLTE 361 DVRTRPEVGELLR
Ric8A_DANRE   237 KILFNVTFDSN 280 TEEMHSHTVNLLG 333 LDRGNKLKETLLPSLNLLTE 374 DVKNRPEVGNALR
Ric8A_CHICK   233 KVLFNITFDSS 276 TEEFHSHTVNLLG 329 LDRGHKLKESLTPVLNLLTE 370 DVKNRPEVGNSLR
Ric8A_XENTR   233 KTLFNITFDIS 276 TEEFHGHTVNLLV 329 LDRGHKLRETLTPVLNLLTE 370 DVKNRPEVGNTLR
Ric8B_DANRE   237 KALFNLTMSDS 277 TEETHSHAINLLS 330 IDKGFNFKEGLTPVLSLLTE 371 DVKERPEIGDTIR
Ric8B_XENTR   220 KALFNVTLDSW 272 TEELHSNTVNLLS 315 IDKGCSYREGLTPVLSLLTE 356 DVSNRPEVGMTVR
Ric8B_CHICK   234 KALFNVTLDSW 276 TEELHSNAINLLS 330 IDKGSSYREGLTPVLSLLTE 361 DVSSRPEVGTTVR
Ric8B_HUMAN   232 KALFNVTVDSW 274 TEELHSNAVNLLS 353 IDKGSSYREGLTPVLSLLTE 304 DVTNRPEVGSTVR
Ric8B_BOVIN   232 KALFNVTVDSW 274 TEELHSNAVNLLS 353 IDKGSSYREGLTPVLSLLTE 304 DVTNRPEVGSTVR
Ric8B_MOUSE   232 KALFNVTVDSW 274 TEELHSNAVNLLS 353 IDKGSSYREGLTPVLSLLTE 304 DVTNRPEVGSTVR
Ric8B_RAT     232 KALFNVTVDSW 274 TEELHSNAVNLLS 353 IDKGSSYREGLTPVLSLLTE 304 DVTNRPEVGSTVR
                  * ***:*.        *** *.:::***     :.:  - :* :-* *.:***     **  ***:*  :*
                     αC5            αb6                    αC7            αA8

Ric8A_RAT     374 NKLVRLMTHLDTDVKRVAAEFLFVLCSESVPRFIKYTGYGNAAGLLAARGLMAGGRPEGQ 433
Ric8A_MOUSE   374 NKLVRLMTHLDTDVKRVAAEFLFVLCSESVPRFIKYTGYGNAAGLLAARGLMAGGRPEGQ 433
Ric8A_HUMAN   375 NKLVRLMTHLDTDVKRVAAEFLFVLCSESVPRFIKYTGYGNAAGLLAARGLMAGGRPEGQ 434
Ric8A_BOVIN   374 NKLVRLMTHLDTDVKRVAAEFLFVLCSESVPRFIKYTGYGNAAGLLAARGLMAGGRPEGQ 433
Ric8A_DANRE   387 NKLVRLMTHIDTDVKHCAAEFLFVLCKESVSRFIKYTGYGNAAGLLAARGLMRGGRDPGH 446
Ric8A_CHICK   383 NKLVRLMTHIDTDVKHCAAEFLFVLCKESVSRFVKYTGYGNAAGLLAARGLMAGGREEGE 442
Ric8A_XENTR   383 NKLVRLMTHVDTDVKHCAAEFLFVLCKENVSRFVKYTGYGNAAGLLAARGLLAGGRGEGR 442
Ric8B_DANRE   383 NKLVRLMTHVDMAVKQGAAEFLFVLCKESVDNLLKYTGYGNAAGLLMARGLLAGGRGETQ 443
Ric8B_XENTR   369 NKLVRLMTHVDLGVKQIAAEFLFVLCKERVDSLLKYTGYGNAAGLLAARGLLAGGRGDRW 428
Ric8B_CHICK   384 NKLVRLMTHVDLGVKQIAAEFLFVLCKERVDSLLKYTGYGNAAGLLAARGLLAGGRGDHW 443
Ric8B_HUMAN   407 NKLVRLMTHVDLGVKQIAAEFLFVLCKERVDSLLKYTGYGNAAGLLAARGLLAGGRGDNW 466
Ric8B_BOVIN   407 NKLVRLMTHVDLGVKQIAAEFLFVLCKERVDSLLKYTGYGNAAGLLAARGLLAGGRGDNW 466
Ric8B_MOUSE   407 NKLVRLMTHVDLGVKQIAAEFLFVLCKERVDSLLKYTGYGNAAGLLAARGLLAGGRGDNW 466
Ric8B_RAT     407 NKLVRLMTHVDLGVKQIAAEFLFVLCKERVDSLLKYTGYGNAAGLLAARGLLAGGRGDNW 466
                  *********:*--**:-*********.* *- ::*****************: ***
                     αB8            αC8      αa9           αb9

Ric8A_RAT     444 EYREAKASINPVTGRVEEKPPNPMEGMTEEQKEHEAMKLVNMFDKLSRHR 493
Ric8A_MOUSE   444 EYREAKASINPVTGRVEEKPPNPMEGMTEEQKEHEAMKLVNMFDKLSRHR 493
Ric8A_HUMAN   445 EYKEAKASINPVTGRVEEKPPNPMEGMTEEQKEHEAMKLVTMFDKLSRNR 494
Ric8A_BOVIN   444 EYKEAKASINPVTGRVEEKPPNPMEGMTEEQKEHEAMKLVNMFDKLSRHR 493
Ric8A_DANRE   457 EYREAKPHINPVTGRVEEEQPNPMEGMTDEQKEYEAMKLVNMFDKLSREQ 506
Ric8A_CHICK   453 EYKEAKPNINPVTGRVEEKLPNPMEGMTEEQKEYEAMKLVNMFDKLSREQ 502
Ric8A_XENTR   453 EYREAKPNINPVTGRVEEKQPNPMDGMTEEQKEYEAMKLVNMFDKLSREQ 502
Ric8B_DANRE   454 EYKSVKPFINPITGHVEDPLPNPLDEMTEEQKEYEAQRLVSMIDELSRKE 503
Ric8B_XENTR   439 EYLLAKPNINLITGHVEEPLPNPMDEMTEEQKEYEAMKLVNMFDKLSREE 488
Ric8B_CHICK   454 EYKSAKPNINLITGHLEEPMPNPMDEMTEEQKEYEAMKLVNMFDKLSRDE 503
Ric8B_HUMAN   477 EYKNAKPNINLITGHLEEPMPNPIDEMTEEQKEYEAMKLVNMLDKLSREE 526
Ric8B_BOVIN   477 EYKNAKPNINLITGHLEEPMPNPIDEMTEEQKEYEAMKLVNMLDKLSREE 526
Ric8B_MOUSE   477 EYKNAKPNINLITGHLEEPMPNPIDEMTEEQKEYEAMKLVNMLDKLSREE 526
Ric8B_RAT     477 EYKNAKPNINLITGHLEEPMPNPIDEMTEEQKEYEAMKLVNMLDKLSREE
                  **  .*  **-:**::*:- ***:: **:****:** :**.*:*:***..
                        RT                                α11
```

Extended Data Figure 9a. Amino acid sequences of Ric-8A and Ric-8B across phylogeny near Gα contact residues. Residue numbers are shown at the start and, for long tracts, the end of subsequences that harbor Ric-8A contacting-residues, highlighted in *green* in the sequence of rat Ric-8A, defined as those that include at least one atom within 4.0 of an atom in Gαi1. Amino acids not identical in rat Ric-8A and rat Ric-8B in *red* in the conservation summary at the bottom of each alignment. Central residues of secondary structural elements are shown below the conservation summary.

```
Gs     31 QKDKQVYRATHRLLLLGAGESGKSTIVKQM 60  212 FQVDKVNFHMFDVGGQRDERRKWIQCFNDVTA 243
Golf  102 REQKRDLQQTHRLLLLGAGESGKSTIVKQM 131 268 FQVDKVNFHMFDVGGQRDERRKWIQCFNDVTA 299
G12    46 ARERRAVRRLVKILLLGAGESGKSTFLKQM 75  214 FVIKKIPFKMVDVGGQRSQRQKWFQCFDGITS 245
G13    39 SREKTYVKRLVKILLLGAGESGKSTFLKQM 68  211 FEIKNVPFKMVDVGGQRSERKRWFECFDSVTS 242
GQ     30 NRDKRDARRELKLLLLGTGESGKSTFIKQM 59  194 FDLQSVIFRMVDVGGQRSERRKWIHCFENVTS 225
G11    30 ERDKRDARRELKLLLLGTGESGKSTFIKQM 59  194 FDLENIIFRMVDVGGQRSERRKWIHCFENVTS 225
GT3    24 QEDAERDARTVKLLLLGAGESGKSTIVKQM 53  189 FSFKDLNFRMFDVGGQRSERKKWIHCFEGVTC 220
GT1    20 KEDAEKDARTVKLLLLGAGESGKSTIVKQM 49  185 FSFKDLNFRMFDVGGQRSERKKWIHCFEGVTC 216
GT2    24 QEDADKEAKTVKLLLLGAGESGKSTIVKQM 53  189 FSVKDLNFRMFDVGGQRSERKKWIHCFEGVTC 220
GO     24 KEDGISAAKDVKLLLLGAGESGKSTIVKQM 53  190 FTFKNLHFRLFDVGGQRSERKKWIHCFEDVTA 221
GI2    24 REDGEKAAREVKLLLLGAGESGKSTIVKQM 53  190 FTFKDLHFKMFDVGGQRSERKKWIHCFEGVTA 221
GI1    24 REDGEKAAREVKLLLLGAGESGKSTIVKQM 53  189 FTFKDLHFKMFDVGGQRSERKKWIHCFEGVTA 220
GI3    24 REDGEKAAKEVKLLLLGAGESGKSTIVKQM 53  189 FTFKELYFKMFDVGGQRSERKKWIHCFEGVTA 220
          .:      - ::****::*******::***         * ...: *::.******.:*::*:.**:.:*.
                   β1  P-loop    α1              β2     β3        Switch II

Gs    268 EALNLFKSIWNNRWLRTISVILFLNK 293  358 YCYPHFTCAVDTENIRRVFNDCRDIIQRMHLRQYELL 394
Golf  324 ESLDLFESIWNNRWLRTISIILFLNK 349  414 YCYPHFTCAVDTENIRRVFNDCRDIIQRMHLKQYELL 450
G12   270 ESMNIFETIVNNKLFFNVSIILFLNK 295  343 PLFHHFTTAIDTENIRFVFHAVKDTILQENLKDIMLQ 379
G13   267 ESLNIFETIVNNRVFSNVSIILFLNK 292  343 PLFHHFTTAIDTENIRFVFHAVKDTILQENLKDIMLQ 379
GQ    250 ESKALFRTIITYPWFQNSSVILFLNK 275  341 PLYHHFTTAINTENIRLVFRDVKDTILHDNLKQLMLQ 377
G11   250 ESKALFRTIITYPWFQHSSVILFLNK 275  323 IIYSHFTCATDTENIRFVFAAVKDTILQLNLKEYNLV 359
GT3   245 ESLHLFNSICNHKYFATTSIVLFLNK 270  318 EIYSHMTCATDTQNVKFVFDAVTDIIIKENLKDCGLF 354
GT1   241 ESLHLFNSICNHRYFATTSIVLFLNK 266  314 EIYSHMTCATDTQNVKFVFDAVTDIIIKENLKDCGLF 350
GT2   245 ESLHLFNSICNHKFFAATSIVLFLNK 270  318 EIYSHMTCATDTQNVKFVFDAVTDIIIKENLKDCGLF 354
GO    246 ESLMLFDSICNNKFFIDTSIILFLNK 271  318 EIYCHMTCATDTNNIQVVFDAVTDIIIANNLRGCGLF 354
GI2   246 ESMKLFDSICNNKWFTDTSIILFLNK 271  319 EIYTHFTCATDTKNVQFVFDAVTDVIIKNNLKDCGLF 355
GI1   245 ESMKLFDSICNNKWFTDTSIILFLNK 270  318 EIYTHFTCATDTKNVQFVFDAVTDVIIKNNLKDCGLF 354
GI3   245 ESMKLFDSICNNKWFTDTSIILFLNK 270  318 EIYTHFTCATDTKNVQFVFDAVTDVIIKNNLKDCGLF 354
          *:  :* :* . - : --*::*****          -  -*:* *-:*:*:: ** ---* *-  :*: --*-
             α3      β5          p1              β6    p2          α5
```

Extended Data Figure 9b. Sequence of rat Gα isoforms within Ric-8A contact regions. Residue numbers are shown at the start and end of subsequences that harbor Ric-8A contacting-residues, highlighted in *green* in the sequence of Gai1, defined as those that include at least one atom within 4.0 of an atom in Ric-8A. Amino acids not identical in Gαi and Gαs are highlighted in *red*, in the conservation summary at the bottom of each alignment. Central residues of secondary structural elements are shown below the conservation summary. Symbols p1 and p2 denote guanine nucleotide purine binding sites formed at the β5-αG and β6-α5 loops, respectively.

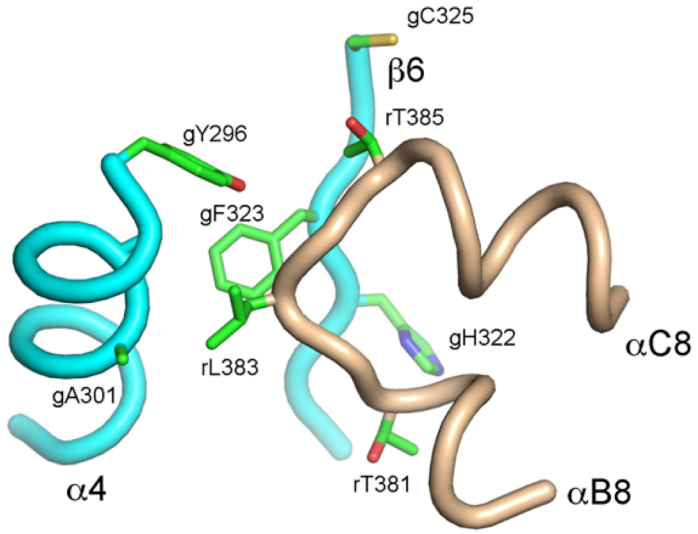

Extended Data Figure 10. Detail of Ric-8A:Gαi1 contact involving Gαi1 α4 and β6 with Ric-8A αB8-αC8. The crystal structure is shown with Gαi1 backbone in *cyan* and Ric-8A backbone in *wheat* with side-chain atom colors, carbon, *green*, nitrogen, *blue*, oxygen, *red* and sulfur, *yellow*. Mutation of rL383 to glutamate reduces GEF activity to 50% that of wild-type Ric-8A.